Strain relaxation, extended defects and doping effects in InxGa1-xN/GaN heterostructures investigated by surface photovoltage

Strain relaxation, extended defects and doping effects in InxGa1-xN/GaN heterostructures investigated by surface photovoltage.

D Cavalcoli[1], A Minj [2,3], M A Fazio[1], A. Cros [4], M. Heuken[5]

[1]Physics and Astronomy Dept. University of Bologna

[2]IMEC, Kapeldreef 75, Leuven 3000, Belgium

[3]KU Leuven, Afdeling Kern- en Stralingsfysica, Celestijnenlaan 200d, Heverlee 3001, Belgium

[4]Institute of Materials Science (ICMUV), Universidad de Valencia, PO Box E-22085, Valencia, Spain

[5]AIXTRON SE Dornkaulstraße 2 52134 Herzogenrath Germany

Corresponding Author:

Prof Daniela Cavalcoli

Physics and Astronomy Dept

University of Bologna

Viale C Berti Pichat 6/II

40127 Bologna

Phone: +39 051 2095116

e-mail: daniela.cavalcoli@unibo.it

e-mail: cavalcoli@bo.infn.it

Strain relaxation, extended defects and doping effects in $In_xGa_{1-x}N$/GaN heterostructures investigated by surface photovoltage.

D Cavalcoli[1], A Minj[2,3], M A Fazio[1], A. Cros[4], M. Heuken[5]

[1]Physics and Astronomy Dept. University of Bologna

[2]IMEC, Kapeldreef 75, Leuven 3000, Belgium

[3]KU Leuven, Afdeling Kern- en Stralingsfysica, Celestijnenlaan 200d, Heverlee 3001, Belgium

[4]Institute of Materials Science (ICMUV), Universidad de Valencia, PO Box E-22085, Valencia, Spain

[5]AIXTRON SE Dornkaulstraße 2 52134 Herzogenrath Germany

Abstract

We have analysed electrical properties of extended defects and interfaces in fully strained and partially relaxed $In_xGa_{1-x}N$/GaN heterostructures by means of Kelvin probe force microscopy and surface photovoltage spectroscopy. The study highlights the role of indium incorporation and Si doping levels on the charge state of extended defects including threading dislocations, V defects and misfit dislocations. Surface potential maps reveal that these defects are associated with a different local work function and thus could remarkably alter electron-hole recombination mechanisms of $In_xGa_{1-x}N$/GaN layers locally. Surface photovoltage spectra clearly demonstrate the role of misfit dislocations and high Si-doping level on interface recombination process. The interplay between Si doping level and In% on the electronic properties of the extended defects has been also clarified.

1. Introduction

III-Nitride alloys uniquely offer tuning of their bandgap from infra-red (0.7 eV) to ultra-violet (6.1 eV) as well as strong anisotropic polarization reaching as high as 0.081 C/m^2. Thanks to their high thermal and mechanical stability, $Al_xGa_{1-x}N$ and

(low-indium content) $In_xGa_{1-x}N$ based optoelectronic devices have already approached commercial applications. While white, blue and ultra-violet light emitting diodes (LEDs) are well-known examples [1], AlGaN/GaN based high electron mobility transistors [2] are considered serious contenders for replacing vacuum tubes in radio-frequency (RF) electronics for multitude of applications. Apart from light emitting applications, $In_xGa_{1-x}N$-based structures might as well be highly promising for THz detection based on inter-subband absorption in the quantum wells and for multijunction solar cells in tandem with Si [3]. However, special attention towards the material characteristics is required, as fundamental material issues still need to be understood and resolved.

Due to the large mismatch in their lattice constants and thermal coefficient with respect to the commonly used growth substrates (Sapphire Al_2O_3, Si(111) and SiC(0006)), generation of extended defects which accommodate lattice and thermal strain is unavoidable [4]. As a result, the most commonly occurring defects include misfit dislocations (MDs), threading dislocations (TDs), stacking faults (SFs), stacking mismatch boundaries, inversion domain boundaries, and others. While not being limited to the substrate, also the strain arising in ternary alloys, especially $In_xGa_{1-x}N$ and $In_xAl_{1-x}N$ grown on mismatched GaN buffer layer, results in formation of V-defects and SFs, phase separation, chemical ordering etc. The most common type of V-defects or inverted pyramidal structures in nitrides, i.e. the ones that terminate the threading dislocations at the surface, have been deeply investigated before for both ternary alloys [5]. Stacking mismatch boundaries have also been reported. In these defects, the proximity of similar V-defect structures form characteristic trenches resulting in local strain relaxation. [6]. The primary mechanism of strain relaxation in hexagonal systems is, however, through dislocation glide on slip system. In the absence of net shear force in biaxially strained $In_xGa_{1-x}N$ layers, dislocation glide is only active for the two pyramidal slip systems, <11-23>{11-22} and <1-101>{1-102} [7], favorably for the former resulting in the

formation of a trigonal misfit dislocation network at the $In_xGa_{1-x}N$ /GaN interface or the crosshatch pattern [8].

While these extended defects have been intensively studied through structural investigation, their role in electron-hole recombination mechanisms is still quite debated. These mechanisms play a major role in current transport and have a relative impact on device reliability and device electrical and optical properties. To cite some examples, the insertion of an $In_xGa_{1-x}N$/GaN superlattice with a lower In content before the growth of $In_xGa_{1-x}N$/GaN multiple quantum wells (MQWs) is known to increase the efficiency of LEDs; however the actual mechanism is still not completely clear [9]. The beneficial effect of this buffer layer has been attributed to its ultralow TD density; it enables the capability of this layer to relax strain due to the absorption of MDs in a region within few nanometers from the interface, leading to a high-quality overlying GaN epilayer [10]. Cathodoluminescence and Raman measurements have demonstrated that the potential barrier formed by V-pits during the low-temperature growth of $In_xGa_{1-x}N$/GaN superlattice dramatically increases the internal quantum efficiency of $In_xGa_{1-x}N$ quantum wells by suppressing non-radiative recombination at TDs [11]. Thus, a controlled amount of TDs and V-pits seems to play a beneficial role in the enhancement of LED efficiency [12]. The picture is even more complex in solar cells. Up to now the experimentally obtained efficiency is lower than the expected one, likely due to charge localization phenomena induced by native polarization effects [13] and strain-generated defects in In-containing nitride heterostructures.

The study of electron-hole recombination at dislocations is therefore of major importance to understand the mechanisms that could result in efficiency improvement of III-N based devices.

Surface band bending and recombination properties due local defects, space charge regions and surface states have been previously explored in (Al,GaN) using Kelvin probe force microscopy (KPFM) and surface photovoltage spectroscopy [14][15][16].

In the present contribution we focus on threading dislocations, V-defects and misfit dislocations in $In_xGa_{1-x}N$/GaN heterostructures with varying In concentrations and different Si doping level. Using these techniques, we will clarify the role of extended defects on electron-hole recombination mechanisms through a correlative surface potential and surface photovoltage spectroscopy study.

2. Experimentals

We have investigated two sets of $In_xGa_{1-x}N$(50 nm)/GaN(3 μm) heterostructures epitaxially grown on sapphire, one Si doped, labelled d-, the other nominally undoped, labelled u. Indium concentration has been varied in order to cover both fully strained and partially relaxed layers.

All the layers have been grown by AIXTRON Metal Organic Chemical Vapour Deposition Close-Coupled Showerhead reactor. The structural details, indium concentration and carrier density for Si-doped samples are listed in Table 1, while the deposition details are reported elsewhere [17]. Indium content has been extracted by applying Vegard's law to high-resolution X-ray powder diffraction (XRD) analysis, while the carrier density of the layers has been evaluated by electrochemical capacitance-voltage measurements (ECV). ECV was preferentially employed due to the difficulty in fabricating Schottky contacts on In-rich $In_xGa_{1-x}N$ layers with high density of n-type doping [18].

Surface potential is measured locally by KPFM within an atomic force microscope (AFM) operating in tapping mode [19]. KPFM allows for two-dimensional mapping with resolution in the nanometer range of the contact potential difference (CPD) between a conductive tip and the sample. When the tip oscillates, in addition to the atomic force, a long-range electrostatic force exists between the tip and sample, which is determined by the CPD between them. This force is detected by applying an ac voltage to the tip and using a lock-in amplifier. The electrostatic force is nullified when the CPD is completely compensated by a dc voltage applied to the tip. In this case, the CPD is equal to the applied dc voltage.

Surface Photovoltage spectra is measured by using a MIS (Metal Insulator Semiconductor) structure. The surface of a semiconductor, due to the presence of surface related –charged defect states, contains uncompensated impurities which creates a space charge region. Under optical excitation, photo generated excess carriers redistribute within the surface or the bulk, creating a change in the surface potential. The SPV is defined as the illumination induced change of the surface potential, its variation as a function of the impinging photon energy allows for the extraction of absorption –related electronic transitions. [20].

Table 1.

Table 1. In-concentration, free carrier densities, defects in Si-doped (d) and nominally undoped (u) $In_xGa_{1-x}N$/GaN heterostructures. In the last column the detection of misfit dislocations (MDs) at the $In_xGa_{1-x}N$/GaN interface through the observation of trigonal network in 5x5 μm^2 morphology is assessed.

Sample	**In (%)**	**Carrier density ($\times 10^{18}$ cm^{-3})**	**Si doping (undoped, Low, Medium, High)**	MDs
dA	14.0	7	L Si	no
dB	19.0	10	L Si	yes
dC	22.0	40	M Si	yes
dD	19.3	90	H Si	yes
dE	19.3	90	H Si	yes
uF	15.6	-	undoped	no
uG	16.3	-	undoped	no
uH	18.0	-	undoped	yes

Indium percentage in the Si-doped $In_xGa_{1-x}N$ top layers ranges from 14% to 22%, where the n-type carrier density differs in all the layers. Here, the samples are labelled in alphabetical order showing increasing carrier density. The samples with indium content lower than 17% are fully strained heterostructures and present no evidence of misfit dislocations at the interface. The $In_xGa_{1-x}N$ layer thickness here is strictly below the critical thickness, as concluded by following the analytical

modelling from ref. [21] on strain relaxation through a pyramidal slip system on $In_xGa_{1-x}N$/GaN heterostructures. In a previous report [22], it has been demonstrated by geometric phase analysis of the $In_xGa_{1-x}N$/GaN interface that they indeed exhibit a fully strained pseudomorphic structure. Meanwhile, the samples with In-content above 17% are considered as a partially-relaxed matrix and a variety of lattice defects, including misfit dislocations, trenches etc., have been observed in topography and in transmission electron microscopy (TEM) analysis.

In order to study the electrical properties of extended defects in terms of local surface band bending representing their donor/acceptor behaviour, the surface work function (WF) was mapped over the different samples by measuring the contact potential difference (CPD) by Kelvin probe force microscopy (KPFM). Here, CPD is defined as

$$e \cdot CPD = WF\ (tip) - WF\ (sample\ surface) \quad (1)$$

where e represents the absolute value of the electronic charge. It must be noted that the changes in CPD and work function are of opposite sign here.

Double-pass topography and Amplitude modulation-KPFM measurements were performed in tapping mode. For each scan-line the height profile is obtained in the first pass keeping amplitude constant through a Z-piezo feedback and the latter is implemented in the second pass, as the AFM tip lifts away from the sample surface by Δz (several nanometres) following the previously obtained height profile. An AC bias of 1.5 V at the resonance frequency of the cantilever was used to excite the electrical signal in the second pass, which was nullified by the DC bias servo feedback. Commercial diamond coated Si probes with a resonance frequency of ~210 kHz and a spring constant of ~72 N/m were used. The measurements were performed in air in NT-MDT pro Solver 47.

Absorption related electronic transitions in $In_xGa_{1-x}N$/GaN samples have been determined by surface photovoltage (SPV) spectroscopy measurements. SPV spectra have been acquired using the laboratory-made apparatus described in ref [23] based

on a 500M SPEX spectrometer, a pre-amplifier and an SRS lock-in amplifier, while the measurement is controlled by a LabView-based software. A Xe lamp has been used to inject photons. As the impinging photon flux varies as a function of the wavelength, the SPV raw data (SPV_{raw}) have been normalized to the photon flux Φ measured by a pyroelectric sensor and plotted as a function of the photon energy hv as follows:

$$SPV_{norm} = \frac{SPV_{raw}}{\Phi/_{hv}} \qquad (2)$$

The penetration depth of the photon beam within the samples can be estimated as α^{-1}, where α is the absorption coefficient and it varies as a function of the photon energy. Experimental values of α (red curve) and α^{-1} (black line) of $In_xGa_{1-x}N$ as a function of the photon energy, obtained by ellipsometry measurements [24], are shown in fig. 1a. It can be noticed that, for photon energies $hv \gg E_{g,GaN}$, α^{-1} becomes lower than 100 nm, thus photon absorption occurs mainly in the $In_xGa_{1-x}N$ top layer, whose thickness is 50 nm; when $hv \geq E_{g,GaN}$, absorption occurs mainly at the $In_xGa_{1-x}N$/GaN interface; while, when $hv < E_{g,GaN}$, absorption takes place mainly in the GaN buffer layer, thus in this spectral range SPV measurements are sensitive to defect-related electronic transitions in the GaN buffer layer.

3. Results

3.1 Surface potential maps.

3.1.1 Surface Morphology.

The band structure of the $In_xGa_{1-x}N$/GaN interface of Si-doped set has been simulated by numerically solving self-consistently Schrödinger-Poisson equations (NEXTNANO software [25]), with $In_xGa_{1-x}N$ and GaN offsets extracted from literature [26]. Fig 1b shows the band simulation for samples dA and dB, where sample dB is shown as representative as for all the other samples of this set, as they show similar simulated band diagrams. The difference between the band diagrams

of dA and dB is related to the fact that dA is the only fully strained sample, while the others are partially relaxed (see Table 1). Similar results have been obtained by the authors of ref [27]. A higher surface barrier height is obtained for fully strained structure and should be related to the strain-induced negative piezoelectric polarization charge density (as high as $2x10^{13}$ e/cm^2) at the interface, which widens the depletion layer.

Figure 2 (a-e) shows the surface morphology over a 5x5 μm^2 scan area for Si doped samples (from dA to dE) with different indium contents. In all the maps, apart from sample dA (fig 2a), lines running across each other at 60°are clearly visible, and from our analysis they are related to misfit dislocations at the interface creating a crosshatch pattern parallel to the surface [28]. Occurrence of such a crosshatch pattern is due to the strain relaxation in compressively strained heterostructures with hexagonal lattice via dislocation slip on <11-23>{11-22} systems towards the interface. As a result, dislocation lines running along <1-100> with a Burgers vector of a+c or 1/3<11-23> are expected, which were also observed here by TEM images [28]. The contrast for the crosshatch pattern is mainly due to preferential growth along the dislocation line on the steps formed during <11-23>{11-22} slips, which could indicate alteration in growth dynamics. In contrast to what was observed in fig 2 (b-e), fig 2a does not show any evidence of the misfit dislocation pattern, as sample dA, whose In% is below 17%, can be considered fully strained. The root mean square surface roughness has been extracted and plotted as a function of indium content in Figure 2f. The roughness increases with the indium content in correlation with the increase in the underlying crosshatch pattern density. In the roughness estimation, features of higher height, most likely related to indium droplets or localized In-rich $In_xGa_{1-x}N$ overgrowth regions, were not accounted for. The results reported here clearly show the important role of dislocations in strain relaxation and the impact of In on the degradation of the morphological properties of the layers.

3.1.2 Undoped $In_xGa_{1-x}N$ layers (x<0.18): low- and high-density V-defects

Surface electronic properties were analysed by KPFM, as the detection of work function variation could provide insight into alloy inhomogeneity, band bending and surface charge state and distribution. It was implemented on the as-grown undoped sample (uG) straight after its growth without following any surface treatment (for example, native oxide etch). The analysis broadly categorized V-defects into two types; the ones that are related to underlying threading dislocations with a higher density (HD) and the others occurring with a lower density (LD). As seen in the figures 3a and b, they are both associated with positive CPD variation across their cores forming a peak (HD V-defect is indicated by green arrow, LD V-defect by blue arrow in the figure), but they can be distinguished from the difference in the CPD values. This is evidently depicted in the CPD and height profiles comparison across the two types of V-defects in figure 3c. For the HD V-defects occurring with an aerial density ~$2x10^8$ cm^{-2}, net CPD increase at the core on average is around 20 mV and for the LD V-defects with density ~ $1x10^6$ cm^{-2}, it can go as high as 0.24 V. An aerial density in the order of $8/cm^2$ reflects the first type of V-defects (HD V-defects) are associated to TDs, which were also confirmed by TEM analyses, [29]. However, the source of second type of V-defects (LD V-defects) whose density is two order of magnitude lower, remains unclear. For a better clarity over the distribution of LD V-defects, CPD map over a scan area of 20x20 μm^2 is presented in figure 4a. Very importantly, the positive CPD variation across V-defects, which correspond to a negative variation of the work function, here suggests negatively charged space charge region across the underlying TDs or its core. This could be an evidence of positively charged core of V-defects in n-type III-nitrides. Even though it is commonly accepted that extended defects like dislocations are negatively charged in n-type GaN and positively charged only in p-type GaN [30], our observations can be understood considering a huge polarization field at $In_xGa_{1-x}N$/GaN interface and thin $In_xGa_{1-x}N$ layer which have implications on the position of the Fermi level. For undoped heterostructures, in the absence of screening, the Fermi level is very close to the valence band and could even go below the valence band near the interface,

making the neighboring region in $In_xGa_{1-x}N$ heavily or degenerate p-type. This renders the formation of donor vacancies, such as $V_{N,}$ highly favorable including at the dislocation core, thus making it positively charged. This is only true for the lower segment of the V-defect (i.e. dislocation) present exclusively in $In_xGa_{1-x}N$ close to the interface while GaN remains depleted near the interface.

A rough estimation of the dimension of TD segment in a V-defect in $In_xGa_{1-x}N$ layer can be done: with the diameter of V-defects opening at the surface in the range of 50-60 nm as measured by AFM and with the $In_xGa_{1-x}N$ layer thickness of 50nm, their expected dislocation segment length is very small, $l_{TD,InGaN}$ ~ 1 to 7 nm . We also noted that any surface treatment (HCl, 2%HF or Aqua regia) for oxide etch resulted in the widening of the V-defect because of the preferential etching of semi-polar facets of V-defects, reducing $l_{TD,InGaN}$ even further with most of the lengths being reduced to 0 nm. After the oxide etch step, this positive CPD contrast related to V-defect was not observed anymore, which could be ascribed either to the diffusion of negatively charged ions (Cl^- or F^-) to the core or to the etching of a significant part of the dislocation in $In_xGa_{1-x}N$ layer. This is visible in the surface morphology in figure 3d and in the height profile across one of the V-defects. However, KPFM analysis instead showed negatively charged V-defects for such treated-surfaces. This is evident from the CPD map in figure 3e, where for each V-defect a significant local drop in CPD forming dark spots is seen, but with varying magnitudes. Across one such V-defect, a net CPD drop of ~130 mV dispersed over ~380 nm is measured in the CPD profile (figure 3e). We attribute this to be the sign of widely accepted negatively charged dislocation in n-type GaN.

The positively charged high-density and low-density V-defects were observed only in sample uG. As-grown sample uF with lower indium concentration exhibited HD V-defects with no distinguishable contrast in CPD map and LD defects with higher CPD values, where the latter type of defects were associated to trench-like defects (encircled in topography/CPD map presented in fig. 4b/c) instead of V-shape

defects unlike sample uG. The HD V-defects appeared negatively charged only after chemical treatment.

3.1.3 Doped $In_xGa_{1-x}N$ layers ($0.19 \leq x \leq 0.22$): Low density V-defects

In addition to MDs for doped sample dB, defects with a density of ~ $1x10^6$ cm^{-2} (estimated over 40x40 μm^2) were clearly detected in the CPD map as patches with dark contrast (fig. 4f). Magnified topography centered over such defects in fig. 4g reveals them to be localized over microscale circular regions (referred to as "ring-like defect" from here onwards) with diameters up to ~500 nm and are associated to a net drop in CPD value of 0.22 to 0.25 V at the core. As shown in fig 4g, this ring-like defect constitutes a well-defined ring structure elevated in Z height by ~2.7 nm and encloses a V-pit at its center. The broad radial CPD dispersion extending by more than 2 μm from its core suggests these defects are negatively charged. This behavior is reasonable for extended defects acting as electron acceptors for a heavily doped n-type $In_xGa_{1-x}N$ layer. As sample dB has a high In-content (19%), ring-like structure could be due to a local increase of indium content leading to enhanced growth over pre-existing defects of the GaN template. Though both increase in electron affinity at the V-defect {1-101} facets [[31]] and enhanced indium-inclusion in ring-like defect could as well lead to a higher work function [32], their impact on work function spatial distribution around the defect is expected to be localized and limited within the spatial resolution of the measurement technique itself. It is important to note that one must be careful in considering such an increase in the work function equivalent to the spontaneous energy barrier formation due to enhanced indium inclusion often reported for $In_xGa_{1-x}N$/GaN super lattice at V-defects [33][34].

To gain physical insight on the origin of LD defects, GaN template used in the growth of these heterostructures was investigated. Its surface morphology also shows LD V-defects with a density in the range 0.7-1.5x 10^6 cm^{-2} (estimated on area 400 - 3600 μm^2) with diameter varying between 280 to 410 nm (see figure 4h). The density and diameter obtained here are in very good agreement with the ring-like defect in the doped sample. In addition, KPFM analysis also associates these V-

defects with CPD lower than 0.7 V on average with respect to its surrounding (figure 4i), suggesting them to be negatively charged as well. These V-shape defects are most likely to be formed over underlying nano-pipes [35] and/or wide open-core screw dislocations, which are commonly occurring defects in GaN buffer [36][37][38]. In our previous work, we as well observed evidence of nanopipes in the GaN template used for growth of undoped $In_xGa_{1-x}N$ layer in the TEM analysis, however, their density assessment was not possible [29]. Similar low-density values for screw dislocations were obtained by Massabuau et al. in $In_xGa_{1-x}N$(x=0.08)/n-GaN heterostructures[39].

The CPD contrast is prominent at ring-like defects only in the case of heavily doped n-type $In_xGa_{1-x}N$ case, this could be due to Fermi-level pinning at these defects acting as electron traps. Due to low interface polarization charge density arising from strain relaxation via formation of misfit dislocation, n-type free carriers diffuse from heavily doped $In_xGa_{1-x}N$ layer into GaN buffer and get trapped at nanopipes/dislocation cores, thus rendering them negatively charged. This leads to a local upward band bending in GaN at the interface and subsequently to a lower CPD around these defects, as observed.

Comparing figures 4a, c, f and i, which are at the same scale of 20x20 μm^2, KPFM contrast analysis clearly shows local regions with a comparable density corresponding to higher CPD values in undoped $In_xGa_{1-x}N$ layers at LD V-defects and at trenches (fig 4a,c), and with lower CPDs at ring-like defects in doped $In_xGa_{1-x}N$ and at nanopipes in GaN buffer layer (fig 4f,i). The formation mechanism of such defects would require a deep structural investigation by TEM. However, this study is significantly hindered by the fact that these defects occur with a very low density. Based on our statistical comparison done through surface morphology assessment and KPFM contrast analysis, one may link the origin of these peculiar defects (LD V-shape defects, trenches and even ring-like defects) to the presence of underlying nanopipes in GaN template.

3.1.4 Undoped and heavily doped $In_xGa_{1-x}N$ layers (x≥18%): Formation of misfit dislocations

Irrespective of the doping, misfit dislocations start to appear at the interface as In concentration exceeded beyond 18% in $In_xGa_{1-x}N$ for the same nominal thickness of 50 nm. Samples with misfit dislocations are shown in figures 4d-f. Figures 4d and 4e show 20 μm x 20 μm² topography and CPD maps, respectively, for the undoped sample uH. The crosshatch patterns forming misfit dislocations are clearly visible in both types of maps. For the Si doped sample dB, while the morphological pattern related to the MD network is present similar to the undoped case, only negligible CPD changes appear across the MDs in the CPD map (in figure 4f) unlike in sample uH. Therefore, in doped $In_xGa_{1-x}N$ layers, MDs do not create any clear contrast in CPD maps. We can relate this effect to the presence of a high carrier density (in our case, $7x10^{18}$ – $9x10^{19}$ cm^{-3}, as shown in table 1), which is comparable to (as in samples dA and dB) or significantly higher than (as in samples dC-dE) the reported Mott density of ~10^{19} cm^{-3} in GaN [13]. Such high carrier density in doped $In_xGa_{1-x}N$ layers is enough to screen the potential induced by the polarization charge at the interface irrespective of the presence or absence of misfit dislocations. Hence, the surface barrier height over the underlying MD does not strictly depend on the interface charge density and results in a poor contrast in the KPFM image.

3.2 Surface Photovoltage Spectra.

The Si doped $In_xGa_{1-x}N$/GaN samples reported in Table 1 have been investigated by SPV spectroscopy. Figure 5a shows the SPV spectra (raw data) of the doped layers, for different doping level and In content. The spectra have been acquired from the front side of the samples while the backside was grounded. As the most relevant features in an SPV spectrum occur at the energy corresponding to the band gap [23], we can relate the two main features of each spectrum in Figure 4a to the $In_xGa_{1-x}N$ and GaN energy gaps at lower and higher energies, respectively. The SPV spectra show that $In_xGa_{1-x}N$ bandgap decreases for increasing In%, ranging approximately from 2.6 to 2.9 eV; whereas the GaN related peak is located at 3.4 eV for all the

samples. The values of the $In_xGa_{1-x}N$ band gap extracted by the SPV spectra are shown as pink stars in Figure 5b, and they are compared with previous reported results [40] and calculated Vegard's law with different bowing parameters. The band gap values are in agreement with ref [24] mostly with a bowing parameter $b = 1$. The acquisition of all the spectra has been carried out with equal photon intensities, thus the comparison between the spectra shows that the intensity of the SPV measured at the $In_xGa_{1-x}N$ gap threshold decreases when the Si doping level increases, implying that the charge injection and collection efficiency degrades for high doping level. The large electron density of the highly doped layers (around 10^{20} cm^{-3}) promotes recombination with photo-generated holes, decreasing the overall signal.

In addition to the band-gap related features, the spectra in Fig. 5a show a drop of the signal around 3.3 eV, which deepens with higher Si doping. The least magnitude of the drop is seen for sample dA with lowest Si doping concentration and without MDs. The decrease of the SPV signal at photon energies just above the $In_xGa_{1-x}N$ band gap can be related to an interface recombination effect. As shown in Fig. 1a, the inverse of the absorption coefficient, which equals the light penetration depth, decreases for above band gap energies; thus, in this spectral region the SPV signal is related to recombination phenomena at the interface [20]. Therefore, high Si doping corresponds to a higher interface recombination rate, as Si incorporation induces active interface recombination centers. Moreover, both indium content and silicon doping affect the steepness of the $In_xGa_{1-x}N$ gap- related increase. An ideal peak should be a step function that rises precisely at the energy of the bandgap. In real spectra, the signal increases more gradually with a certain slope. This slope can be attributed to the formation of Urbach tails due to a disordered structure [20]. In Fig. 5a, it is visible that the slope decreases as both Si doping and In content increases; indeed, the increment of both elements concentration creates more defects, indium statistical fluctuation or alloy disorder [41],[22] and phase separation [42] leading to a more pronounced Urbach tails.

For comparison, normalized SPV spectra of the undoped $In_xGa_{1-x}N$/GaN samples uF and uH, without and with misfit dislocations, respectively, are reported in Fig. 6a. Similar to the doped samples spectra, the band gap related features at 3.4 eV (GaN) and in the range varying from 2.7 eV to 2.85 eV ($In_xGa_{1-x}N$) for both samples are visible in the spectra. However, the signals appear quite different in the transition range between the two gaps, which corresponds to the interface region. Indeed, a dip occurs in the sample uH at around 3.3 eV. The dip could be related to recombination processes occurring at the $In_xGa_{1-x}N$/GaN interface induced by MDs, while the SPV spectrum of the sample without MDs (uF) does not show a similar drop as in sample dA with least Si doping. Another feature appears in both samples in the form of a band at around 2.2- 2.4 eV in the spectra of Fig 6a. The same feature appears in the SPV spectra in fig 6b, where scans acquired from different spots on the surface of the GaN template are shown. This feature must be related to the yellow band transition (YB) which is very common in GaN and widely reported in literature and is associated to defects present near the surface [43]. It is interesting to note that this transition is not visible in the SPV spectra of the doped samples (fig. 5). This further strengthens our claim of high Si doping and strain induced recombination centers at the interface.

4. Discussion and Conclusions.

We have investigated Misfit dislocations, threading dislocations, V defects and interfaces in $In_xGa_{1-x}N$/GaN heterostructures by surface potential maps and spectra. As mentioned in the introduction section, while these extended defects have been intensively studied through structural investigation, their electron-hole recombination mechanisms are still quite debated. These mechanisms play a major role in current transport and device reliability. We summarize in the following the main results achieved, highlighting the role of In concentration and doping on the defect characteristics:

- The present analysis has allowed us to detect two categories of V-defects in $In_xGa_{1-x}N$/GaN heterostructures appearing in different densities (Low and High, LD, and HD)
- **In undoped $In_xGa_{1-x}N$/GaN heterostructures**, KPFM maps shows that HD **V defects, corresponding to threading dislocations are positively charged**, contrary to what is known for bulk n-type GaN. This is most likely to be due to the position of the Fermi-level of the $In_xGa_{1-x}N$ layer near the interface with GaN, which is very close to the valence band.
- **In partially relaxed $In_xGa_{1-x}N$ layers**, as observed by KPFM, misfit dislocations are associated to a local drop in work function values, thus MDs create potential wells where electron-hole recombination phenomena are enhanced. The effect of misfit dislocations in the enhancement of electron – hole recombination at the $In_xGa_{1-x}N$/GaN heterointerface is also observed by SPV spectra. WF drops at MDs are not revealed by KPFM in highly Si doped samples due to the effect of doping-induced screening.
- LD V-defects appear in AFM and KPFM maps as ring-like defects, likely related to nanopipes in the GaN buffer, they are associated to an increase in the WF values, which in turn creates a potential barrier for mobile charges. This result could explain why V-defects can have beneficial effects in $In_xGa_{1-x}N$: they can prevent electron-hole recombination, resulting in the enhancement of $In_xGa_{1-x}N$ based LED efficiency, as reported by ref [10].
- **High Si doping concentration** enhances the recombination at the hetero-interface and decreases the efficiency in mobile charge separation, as shown by SPV spectra. Lower spreading resistance in the regions around MDs suggest either preferential Si incorporation or improved dopant activation. **High In% and Si doping levels** also lead to an increase of roughness and alloy-disorder which results in large Urbach tails. Misfit dislocations as well promote local crystal disorder increasing Urbach tails.

- The energy gap of $In_xGa_{1-x}N$ has been determined as a function of the In%. The results agree with the Vegard's law with a bowing parameter close to 1.

By summarizing, very high In and Si concentrations play a major role in increasing crystal disorder and interface recombination. The doping level also affect the charge state of the defect.

The results here presented we have contributed to the clarification of defects induced carrier recombination mechanisms in $In_xGa_{1-x}N$/GaN heterostructures.

Acknowledgments

This work was supported by the EU under Project No. PITN-GA-2008-213238 (RAINBOW). Ana Cros acknowledges financial support from project PROMETEO/2018/123 from Generalitat Valenciana and project ENE2016-79282-C5-3-R cofinanced by the Spanish MICINN and FEDER.

Literature

[1] T. Lin, Z.Y. Zhou, Y.M. Huang, K. Yang, B.J. Zhang, Z.C. Feng, Strain-Controlled Recombination in InGaN/GaN Multiple Quantum Wells on Silicon Substrates, Nanoscale Res. Lett. 13 (2018). doi:10.1186/s11671-018-2663-6.

[2] U.K. Mishra, P. Parikh, Y.F. Wu, AlGaN/GaN HEMTs - An overview of device operation and applications, Proc. IEEE. 90 (2002) 1022–1031. doi:10.1109/JPROC.2002.1021567.

[3] H. Kurokawa, M. Kaga, T. Goda, M. Iwaya, T. Takeuchi, S. Kamiyama, I. Akasaki, H. Amano, Multijunction GaInN-based solar cells using a tunnel junction, Appl. Phys. Express. 7 (2014) 034104. doi:10.7567/APEX.7.034104.

[4] K. Safa, P. Capper, Springer Handbook of Electronic and Photonic Materials, 2014. doi:10.1007/s13398-014-0173-7.2.

[5] Y. Chen, T. Takeuchi, H. Amano, I. Akasaki, N. Yamada, Y. Kaneko, S.Y. Wang, Pit formation in GaInN quantum wells, Appl. Phys. Lett. 72 (1998) 710–712.

doi:10.1063/1.120853.

[6] S.C. Tsai, M.J. Li, H.C. Fang, C.H. Tu, C.P. Liu, Efficiency enhancement of blue light emitting diodes by eliminating V-defects from InGaN/GaN multiple quantum well structures through GaN capping layer control, Appl. Surf. Sci. 439 (2018) 1127–1132. doi:10.1016/j.apsusc.2018.01.074.

[7] S. Srinivasan, L. Geng, R. Liu, F.A. Ponce, Y. Narukawa, S. Tanaka, Slip systems and misfit dislocations in InGaN epilayers, Appl. Phys. Lett. 83 (2003) 5187–5189. doi:10.1063/1.1633029.

[8] J. Moneta, M. Siekacz, E. Grzanka, T. Schulz, T. Markurt, M. Albrecht, J. Smalc-Koziorowska, Peculiarities of plastic relaxation of (0001) InGaN epilayers and their consequences for pseudo-substrate application, Appl. Phys. Lett. 113 (2018). doi:10.1063/1.5030190.

[9] C. Haller, J.F. Carlin, G. Jacopin, D. Martin, R. Butté, N. Grandjean, Burying non-radiative defects in InGaN underlayer to increase InGaN/GaN quantum well efficiency, Appl. Phys. Lett. 111 (2017). doi:10.1063/1.5007616.

[10] H.Y. Shih, M. Shiojiri, C.H. Chen, S.F. Yu, C.T. Ko, J.R. Yang, R.M. Lin, M.J. Chen, Ultralow threading dislocation density in GaN epilayer on near-strain-free GaN compliant buffer layer and its applications in hetero-epitaxial LEDs, Sci. Rep. 5 (2015) 1–11. doi:10.1038/srep13671.

[11] S. Zhou, X. Liu, H. Yan, Y. Gao, H. Xu, J. Zhao, Z. Quan, C. Gui, S. Liu, The effect of nanometre-scale V-pits on electronic and optical properties and efficiency droop of GaN-based green light-emitting diodes, Sci. Rep. 8 (2018) 1–12. doi:10.1038/s41598-018-29440-4.

[12] D.H. Kim, Y.S. Park, D. Kang, K.K. Kim, T.Y. Seong, H. Amano, Combined effects of V pits and chip size on the electrical and optical properties of green InGaN-based light-emitting diodes, J. Alloys Compd. 796 (2019) 146–152. doi:10.1016/j.jallcom.2019.05.070.

[13] D.N. Nath, E. Gür, S.A. Ringel, S. Rajan, Molecular beam epitaxy of N-polar InGaN, Appl. Phys. Lett. 97 (2010) 071903. doi:10.1063/1.3478226.

[14] J.W.P. Hsu, H.M. Ng, A.M. Sergent, S.N.G. Chu, Scanning Kelvin force microscopy imaging of surface potential variations near threading dislocations in GaN, Appl. Phys. Lett. 81 (2002) 3579–3581. doi:10.1063/1.1519732.

[15] B.J. Rodriguez, W.-C. Yang, R.J. Nemanich, A. Gruverman, Scanning probe investigation of surface charge and surface potential of GaN-based heterostructures, Appl. Phys. Lett. 86 (2005) 112115. doi:10.1063/1.1869535.

[16] M. Foussekis, J.D. McNamara, A.A. Baski, M.A. Reshchikov, Temperature-dependent Kelvin probe measurements of band bending in *p* -type GaN, Appl. Phys. Lett. 101 (2012) 082104. doi:10.1063/1.4747203.

[17] A. Minj, H. Ben Ammar, A. Cros, N. Garro, P. Gamarra, S.L. Delage, P. Ruterana, Probing the Local Electrical Properties of Al(In,Ga)N by Kelvin Probe Force Microscopy, Phys. Status Solidi Basic Res. 255 (2018) 1–6. doi:10.1002/pssb.201700427.

[18] O Tuna, Understanding and Optimization of InN and high Indium containing InGaN alloys by Metal Organic Chemical Vapor Deposition, Aachen, 2013. https://inis.iaea.org/search/search.aspx?orig_q=RN:45042262.

[19] M. Nonnenmacher, M.P. O'Boyle, H.K. Wickramasinghe, Kelvin probe force microscopy, Appl. Phys. Lett. 58 (1991) 2921–2923. doi:10.1063/1.105227.

[20] L. Kronik, Y. Shapira, Surface photovoltage phenomena: Theory, experiment, and applications, Surf. Sci. Rep. (1999). doi:10.1016/S0167-5729(99)00002-3.

[21] D. Holec, P.M.F.J. Costa, M.J. Kappers, C.J. Humphreys, Critical thickness calculations for InGaN/GaN, J. Cryst. Growth. 303 (2007) 314–317. doi:10.1016/j.jcrysgro.2006.12.054.

[22] A. Minj, M.F. Romero, Y. Wang, Tuna, M. Feneberg, R. Goldhahn, G. Schmerber, P. Ruterana, C. Giesen, M. Heuken, Stimulated emission via electron-hole plasma recombination in fully strained single InGaN/GaN heterostructures, Appl. Phys. Lett. 109 (2016). doi:10.1063/1.4968799.

[23] D. Cavalcoli, M.A. Fazio, Electronic transitions in low dimensional semiconductor structures measured by surface photovoltage spectroscopy,

Mater. Sci. Semicond. Process. 92 (2019) 28–38. https://www.sciencedirect.com/science/article/pii/S1369800118304177.

[24] S.A. Kazazis, E. Papadomanolaki, M. Androulidaki, M. Kayambaki, E. Iliopoulos, Optical properties of InGaN thin films in the entire composition range, J. Appl. Phys. 123 (2018). doi:10.1063/1.5020988.

[25] nextnano, (n.d.). https://www.nextnano.de/.

[26] L. Dong, First Principles Study of Band Offsets and Band Bending of InxGa1-xN / GaN and Zn1-xBexO / ZnO Heterostructures and Quantum Wells, University of Connecticut Graduate School, 2013.

[27] X. Sun, X. Wang, S. Liu, P. Wang, D. Wang, X. Zheng, L. Sang, M. Sumiya, S. Ueda, M. Li, J. Zhang, W. Ge, B. Shen, Determination of the transition point from electron accumulation to depletion at the surface of in<inf>x</inf>Ga<inf>1-</inf><inf>x</inf>N films, Appl. Phys. Express. 11 (2018). doi:10.7567/APEX.11.021001.

[28] Q.T. Li, A. Minj, M.P. Chauvat, J. Chen, P. Ruterana, Interface dislocations in InxGa1–xN/GaN heterostructures, Phys. Status Solidi Appl. Mater. Sci. 214 (2017) 1–5. doi:10.1002/pssa.201600442.

[29] A. Minj, D. Cavalcoli, G.R. Mutta Popuri, A. Vilalta-Clemente, P. Ruterana, A. Cavallini, Electrical properties of extended defects in III-nitrides, Acta Mater. 89 (2015) 290–297. doi:10.1016/j.actamat.2015.01.061.

[30] D. Cherns, C.G. Jiao, Electron Holography Studies of the Charge on Dislocations in GaN, Phys. Rev. Lett. 87 (2001) 205504. doi:10.1103/PhysRevLett.87.205504.

[31] A.L. Rosa, J. Neugebauer, First-principles calculations of the structural and electronic properties of clean GaN (0001) surfaces, Phys. Rev. B. 73 (2006) 205346. doi:10.1103/PhysRevB.73.205346.

[32] P.G. Moses, M. Miao, Q. Yan, C.G. Van de Walle, Hybrid functional investigations of band gaps and band alignments for AlN, GaN, InN, and InGaN, J. Chem. Phys. 134 (2011) 084703. doi:10.1063/1.3548872.

Formatted: Italian (Italy)

[33] A. Hangleiter, F. Hitzel, C. Netzel, D. Fuhrmann, U. Rossow, G. Ade, P. Hinze, Suppression of Nonradiative Recombination by V-Shaped Pits in GaInN / GaN Quantum Wells Produces a Large Increase in the Light Emission Efficiency, Phys. Rev. Lett. 95 (2005) 127402. doi:10.1103/PhysRevLett.95.127402.

[34] A. Kaneta, M. Funato, Y. Kawakami, Nanoscopic recombination processes in InGaN/GaN quantum wells emitting violet, blue, and green spectra, Phys. Rev. B. 78 (2008) 125317. doi:10.1103/PhysRevB.78.125317.

[35] Z. Liliental-Weber, Y. Chen, S. Ruvimov, J. Washburn, Formation Mechanism of Nanotubes in GaN, Phys. Rev. Lett. 79 (1997) 2835–2838. doi:10.1103/PhysRevLett.79.2835.

[36] W. Qian, G.S. Rohrer, M. Skowronski, K. Doverspike, L.B. Rowland, D.K. Gaskill, Open-core screw dislocations in GaN epilayers observed by scanning force microscopy and high-resolution transmission electron microscopy, Appl. Phys. Lett. 67 (1995) 2284–2286. doi:10.1063/1.115127.

[37] I. Arslan, N.D. Browning, Role of Oxygen at Screw Dislocations in GaN, Phys. Rev. Lett. 91 (2003) 165501. doi:10.1103/PhysRevLett.91.165501.

[38] S. Usami, N. Mayama, K. Toda, A. Tanaka, M. Deki, S. Nitta, Y. Honda, H. Amano, Direct evidence of Mg diffusion through threading mixed dislocations in GaN p–n diodes and its effect on reverse leakage current, Appl. Phys. Lett. 114 (2019) 232105. doi:10.1063/1.5097767.

[39] F.C.P. Massabuau, P. Chen, M.K. Horton, S.L. Rhode, C.X. Ren, T.J. O'Hanlon, A. Kovács, M.J. Kappers, C.J. Humphreys, R.E. Dunin-Borkowski, R.A. Oliver, Carrier localization in the vicinity of dislocations in InGaN, J. Appl. Phys. 121 (2017). doi:10.1063/1.4973278.

[40] S. Pandey, D. Cavalcoli, A. Cavallini, Band bowing and Si donor levels in InGaN layers investigated by surface photo voltage spectroscopy, Appl. Phys. Lett. 102 (2013) 142101. doi:10.1063/1.4799658.

[41] M. Auf der Maur, A. Pecchia, G. Penazzi, W. Rodrigues, A. Di Carlo, Efficiency

Drop in Green InGaN / GaN Light Emitting Diodes: The Role of Random Alloy Fluctuations, Phys. Rev. Lett. 116 (2016) 027401. doi:10.1103/PhysRevLett.116.027401.

[42] P. Ruterana, F. Deniel, Observation of ordering and phase separation in InxGa1−xN layers, Mater. Sci. Eng. B. 59 (1999) 186–190. doi:10.1016/S0921-5107(98)00408-5.

[43] M.A. Reshchikov, J.D. McNamara, H. Helava, A. Usikov, Y. Makarov, Two yellow luminescence bands in undoped GaN, Sci. Rep. 8 (2018) 1–11. doi:10.1038/s41598-018-26354-z.

[44] W. Shan, W. Walukiewicz, J. Wu, K.M. Yu, J.W. Ager, S.X. Li, E.E. Haller, J.F. Qeisz, D.J. Friedman, S.R. Kurtz, Band-gap bowing effects in BxGa1-xAs alloys, J. Appl. Phys. 93 (2003) 2696–2699. doi:10.1063/1.1540230.

[45] J. Wu, W. Walukiewicz, K.M. Yu, J.W. Ager, E.E. Haller, H. Lu, W.J. Schaff, Y. Saito, Y. Nanishi, Unusual properties of the fundamental band gap of InN, Appl. Phys. Lett. 80 (2002) 3967–3969. doi:10.1063/1.1482786.

[46] I. Gorczyca, T. Suski, N.E. Christensen, A. Svane, Size effects in band gap bowing in nitride semiconducting alloys, Phys. Rev. B. 83 (2011) 153301. doi:10.1103/PhysRevB.83.153301.

Figure Captions

Figure 1. a) Measured $In_xGa_{1-x}N$ absorption coefficient α (blue curve) and penetration depth α^{-1} (black curve) vs. photon energy. b) Band simulations at the $In_xGa_{1-x}N$/GaN interface for doped sample dA (In content 14%, fully strained) and doped sample dB (In content 19%, relaxed).

Figure 2. Morphology maps of Si doped $In_xGa_{1-x}N$/GaN samples a) dA, 14% In, b) dB, 19% In c) dC, 22.0% In d) dD 19.3% In and e) dE 19.3% In. f) Roughness extracted from the morphology maps. The orange curve is a guide for the eye.

Figure 3. Surface morphologies (a, d) and their corresponding CPD maps (b, e) of the as-grown and oxide-etched undoped sample uG, respectively. (c, f) Similarly, height and CPD profiles across three V-defects (two HD V-defects indicated in green arrow and 1 LD V-defect in blue) for as-grown and a single V-defect for as-grown and oxide-etched sample. Two LD and one HD V-defects are encircled as well for better clarity. The height profile does not pass through the second HD V-defect and therefore it is not indicated in green arrow.

Figure 4. Comparative CPD maps over 20x20 μm^2 scan area of undoped samples uG (a) and uF (c) without MDs, and uH (e) with MDs, doped sample dB (f) and GaN template used for growth (i). Respective topographies (b, d, h) displayed on the left of the CPD maps (c, e, i) correspond to samples uF, uH and GaN template. GaN morphology shows small V-pits and large V-pits. The small V-pits are indicated by green arrows. (g) Surface morphology (left), CPD map (right) and CPD/Height profiles across a ring-like defect indicated in dashed line. MD line directions along the three <1-100> directions are indicated in (d) and (f).

Figure 5. a) SPV spectra acquired by Xe lamp of Si doped $In_xGa_{1-x}N$/GaN samples (see Table 1) from front of the structure. b) Calculated energy gap values of $In_xGa_{1-x}N$ layers for different bowing parameters (lines) and our new results (pink stars) compared with earlier reported results in: [44][45][46][40][24].

Figure 6. a) Normalised spectra of samples uH (black line) and uF (orange line) as a function of photon energy. b) GaN buffer layer normalised spectra acquired in different spots of the surface.

***Highlights (for review)**

Highlights

Positively charged threading dislocations in undoped $In_xGa_{1-x}N$/GaN.

Potential wells at misfit dislocations at $In_xGa_{1-x}N$/GaN enhance electron-hole recombination.

V- defects in $In_xGa_{1-x}N$ associated to potential barriers for mobile charges prevent electron-hole recombination.

*Graphical Abstract (for review)

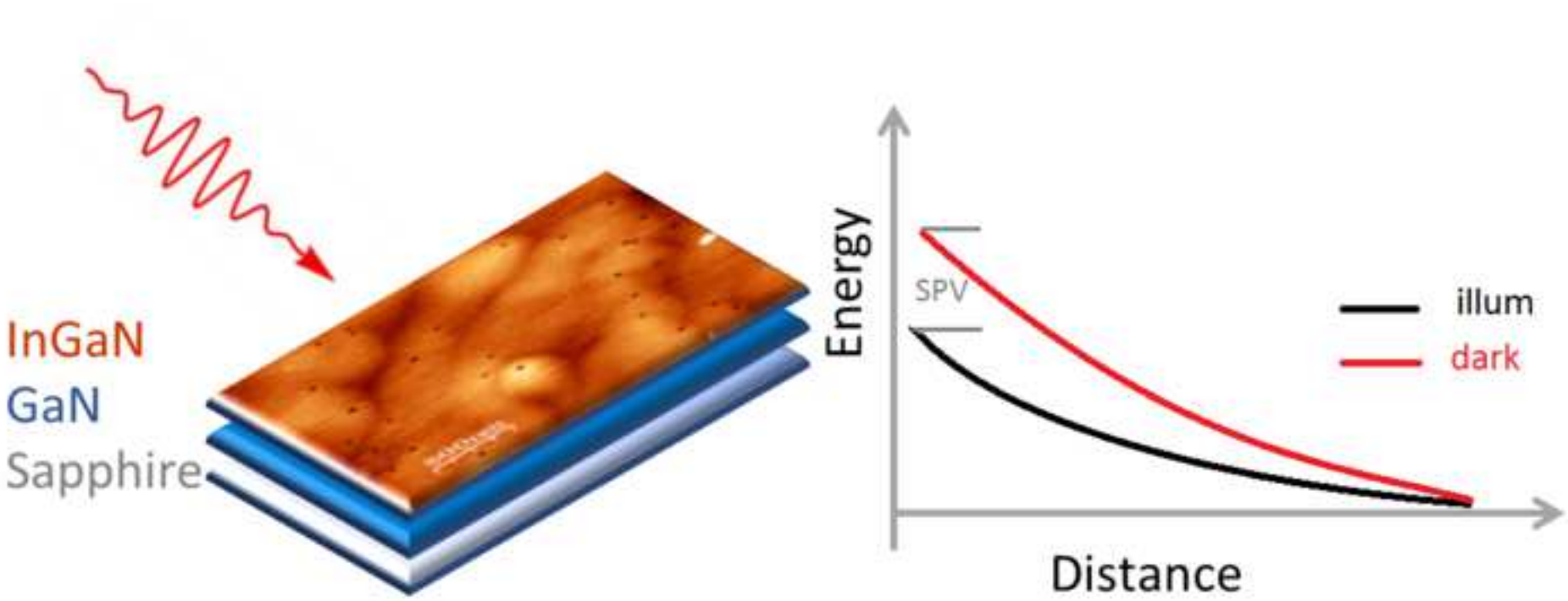

Strain relaxation, extended defects and doping effects in InxGa1-xN/GaN heterostructures investigated by surface photovoltage.

D Cavalcoli[1], A Minj [2,3], M A Fazio[1], A. Cros [4], M. Heuken[5]

[1]Physics and Astronomy Dept. University of Bologna

[2]IMEC, Kapeldreef 75, Leuven 3000, Belgium

[3]KU Leuven, Afdeling Kern- en Stralingsfysica, Celestijnenlaan 200d, Heverlee 3001, Belgium

[4]Institute of Materials Science (ICMUV), Universidad de Valencia, PO Box E-22085, Valencia, Spain

[5]AIXTRON SE Dornkaulstraße 2 52134 Herzogenrath Germany

Corresponding Author:

Prof Daniela Cavalcoli

Physics and Astronomy Dept

University of Bologna

Viale C Berti Pichat 6/II

40127 Bologna

Phone: +39 051 2095116

e-mail: daniela.cavalcoli@unibo.it

e-mail: cavalcoli@bo.infn.it

Strain relaxation, extended defects and doping effects in $In_xGa_{1-x}N$/GaN heterostructures investigated by surface photovoltage.

D Cavalcoli[1], A Minj[2,3], M A Fazio[1], A. Cros[4], M. Heuken[5]

[1]Physics and Astronomy Dept. University of Bologna

[2]IMEC, Kapeldreef 75, Leuven 3000, Belgium

[3]KU Leuven, Afdeling Kern- en Stralingsfysica, Celestijnenlaan 200d, Heverlee 3001, Belgium

[4]Institute of Materials Science (ICMUV), Universidad de Valencia, PO Box E-22085, Valencia, Spain

[5]AIXTRON SE Dornkaulstraße 2 52134 Herzogenrath Germany

Abstract

We have analysed electrical properties of extended defects and interfaces in fully strained and partially relaxed $In_xGa_{1-x}N$/GaN heterostructures by means of Kelvin probe force microscopy and surface photovoltage spectroscopy. The study highlights the role of indium incorporation and Si doping levels on the charge state of extended defects including threading dislocations, V defects and misfit dislocations. Surface potential maps reveal that these defects are associated with a different local work function and thus could remarkably alter electron-hole recombination mechanisms of $In_xGa_{1-x}N$/GaN layers locally. Surface photovoltage spectra clearly demonstrate the role of misfit dislocations and high Si-doping level on interface recombination process. The interplay between Si doping level and In% on the electronic properties of the extended defects has been also clarified.

1. Introduction

III-Nitride alloys uniquely offer tuning of their bandgap from infra-red (0.7 eV) to ultra-violet (6.1 eV) as well as strong anisotropic polarization reaching as high as 0.081 C/m^2. Thanks to their high thermal and mechanical stability, $Al_xGa_{1-x}N$ and

(low-indium content) $In_xGa_{1-x}N$ based optoelectronic devices have already approached commercial applications. While white, blue and ultra-violet light emitting diodes (LEDs) are well-known examples [1], AlGaN/GaN based high electron mobility transistors [2] are considered serious contenders for replacing vacuum tubes in radio-frequency (RF) electronics for multitude of applications. Apart from light emitting applications, $In_xGa_{1-x}N$-based structures might as well be highly promising for THz detection based on inter-subband absorption in the quantum wells and for multijunction solar cells in tandem with Si [3]. However, special attention towards the material characteristics is required, as fundamental material issues still need to be understood and resolved.

Due to the large mismatch in their lattice constants and thermal coefficient with respect to the commonly used growth substrates (Sapphire Al_2O_3, Si(111) and SiC(0006)), generation of extended defects which accommodate lattice and thermal strain is unavoidable [4]. As a result, the most commonly occurring defects include misfit dislocations (MDs), threading dislocations (TDs), stacking faults (SFs), stacking mismatch boundaries, inversion domain boundaries, and others. While not being limited to the substrate, also the strain arising in ternary alloys, especially $In_xGa_{1-x}N$ and $In_xAl_{1-x}N$ grown on mismatched GaN buffer layer, results in formation of V-defects and SFs, phase separation, chemical ordering etc. The most common type of V-defects or inverted pyramidal structures in nitrides, i.e. the ones that terminate the threading dislocations at the surface, have been deeply investigated before for both ternary alloys [5]. Stacking mismatch boundaries have also been reported. In these defects, the proximity of similar V-defect structures form characteristic trenches resulting in local strain relaxation. [6]. The primary mechanism of strain relaxation in hexagonal systems is, however, through dislocation glide on slip system. In the absence of net shear force in biaxially strained $In_xGa_{1-x}N$ layers, dislocation glide is only active for the two pyramidal slip systems, <11-23>{11-22} and <1-101>{1-102} [7], favorably for the former resulting in the

formation of a trigonal misfit dislocation network at the $In_xGa_{1-x}N$ /GaN interface or the crosshatch pattern [8].

While these extended defects have been intensively studied through structural investigation, their role in electron-hole recombination mechanisms is still quite debated. These mechanisms play a major role in current transport and have a relative impact on device reliability and device electrical and optical properties. To cite some examples, the insertion of an $In_xGa_{1-x}N$/GaN superlattice with a lower In content before the growth of $In_xGa_{1-x}N$/GaN multiple quantum wells (MQWs) is known to increase the efficiency of LEDs; however the actual mechanism is still not completely clear [9]. The beneficial effect of this buffer layer has been attributed to its ultralow TD density; it enables the capability of this layer to relax strain due to the absorption of MDs in a region within few nanometers from the interface, leading to a high-quality overlying GaN epilayer [10]. Cathodoluminescence and Raman measurements have demonstrated that the potential barrier formed by V-pits during the low-temperature growth of $In_xGa_{1-x}N$/GaN superlattice dramatically increases the internal quantum efficiency of $In_xGa_{1-x}N$ quantum wells by suppressing non-radiative recombination at TDs [11]. Thus, a controlled amount of TDs and V-pits seems to play a beneficial role in the enhancement of LED efficiency [12]. The picture is even more complex in solar cells. Up to now the experimentally obtained efficiency is lower than the expected one, likely due to charge localization phenomena induced by native polarization effects [13] and strain-generated defects in In-containing nitride heterostructures.

The study of electron-hole recombination at dislocations is therefore of major importance to understand the mechanisms that could result in efficiency improvement of III-N based devices.

Surface band bending and recombination properties due local defects, space charge regions and surface states have been previously explored in (Al,GaN) using Kelvin probe force microscopy (KPFM) and surface photovoltage spectroscopy [14][15][16].

In the present contribution we focus on threading dislocations, V-defects and misfit dislocations in $In_xGa_{1-x}N$/GaN heterostructures with varying In concentrations and different Si doping level. Using these techniques, we will clarify the role of extended defects on electron-hole recombination mechanisms through a correlative surface potential and surface photovoltage spectroscopy study.

2. Experimentals

We have investigated two sets of $In_xGa_{1-x}N$(50 nm)/GaN(3 μm) heterostructures epitaxially grown on sapphire, one Si doped, labelled d-, the other nominally undoped, labelled u. Indium concentration has been varied in order to cover both fully strained and partially relaxed layers.

All the layers have been grown by AIXTRON Metal Organic Chemical Vapour Deposition Close-Coupled Showerhead reactor. The structural details, indium concentration and carrier density for Si-doped samples are listed in Table 1, while the deposition details are reported elsewhere [17]. Indium content has been extracted by applying Vegard's law to high-resolution X-ray powder diffraction (XRD) analysis, while the carrier density of the layers has been evaluated by electrochemical capacitance-voltage measurements (ECV). ECV was preferentially employed due to the difficulty in fabricating Schottky contacts on In-rich $In_xGa_{1-x}N$ layers with high density of n-type doping [18].

Surface potential is measured locally by KPFM within an atomic force microscope (AFM) operating in tapping mode [19]. KPFM allows for two-dimensional mapping with resolution in the nanometer range of the contact potential difference (CPD) between a conductive tip and the sample. When the tip oscillates, in addition to the atomic force, a long-range electrostatic force exists between the tip and sample, which is determined by the CPD between them. This force is detected by applying an ac voltage to the tip and using a lock-in amplifier. The electrostatic force is nullified when the CPD is completely compensated by a dc voltage applied to the tip. In this case, the CPD is equal to the applied dc voltage.

Surface Photovoltage spectra is measured by using a MIS (Metal Insulator Semiconductor) structure. The surface of a semiconductor, due to the presence of surface related –charged defect states, contains uncompensated impurities which creates a space charge region. Under optical excitation, photo generated excess carriers redistribute within the surface or the bulk, creating a change in the surface potential. The SPV is defined as the illumination induced change of the surface potential, its variation as a function of the impinging photon energy allows for the extraction of absorption –related electronic transitions. [20].

Table 1.

Table 1. In-concentration, free carrier densities, defects in Si-doped (d) and nominally undoped (u) $In_xGa_{1-x}N$/GaN heterostructures. In the last column the detection of misfit dislocations (MDs) at the $In_xGa_{1-x}N$/GaN interface through the observation of trigonal network in 5x5 μm^2 morphology is assessed.

Sample	**In (%)**	**Carrier density ($\times 10^{18}$ cm^{-3})**	**Si doping (undoped, Low, Medium, High)**	MDs
dA	14.0	7	L Si	no
dB	19.0	10	L Si	yes
dC	22.0	40	M Si	yes
dD	19.3	90	H Si	yes
dE	19.3	90	H Si	yes
uF	15.6	-	undoped	no
uG	16.3	-	undoped	no
uH	18.0	-	undoped	yes

Indium percentage in the Si-doped $In_xGa_{1-x}N$ top layers ranges from 14% to 22%, where the n-type carrier density differs in all the layers. Here, the samples are labelled in alphabetical order showing increasing carrier density. The samples with indium content lower than 17% are fully strained heterostructures and present no evidence of misfit dislocations at the interface. The $In_xGa_{1-x}N$ layer thickness here is strictly below the critical thickness, as concluded by following the analytical

modelling from ref. [21] on strain relaxation through a pyramidal slip system on $In_xGa_{1-x}N$/GaN heterostructures. In a previous report [22], it has been demonstrated by geometric phase analysis of the $In_xGa_{1-x}N$/GaN interface that they indeed exhibit a fully strained pseudomorphic structure. Meanwhile, the samples with In-content above 17% are considered as a partially-relaxed matrix and a variety of lattice defects, including misfit dislocations, trenches etc., have been observed in topography and in transmission electron microscopy (TEM) analysis.

In order to study the electrical properties of extended defects in terms of local surface band bending representing their donor/acceptor behaviour, the surface work function (WF) was mapped over the different samples by measuring the contact potential difference (CPD) by Kelvin probe force microscopy (KPFM). Here, CPD is defined as

$$e \cdot CPD = WF\ (tip) - WF\ (sample\ surface) \quad (1)$$

where e represents the absolute value of the electronic charge. It must be noted that the changes in CPD and work function are of opposite sign here.

Double-pass topography and Amplitude modulation-KPFM measurements were performed in tapping mode. For each scan-line the height profile is obtained in the first pass keeping amplitude constant through a Z-piezo feedback and the latter is implemented in the second pass, as the AFM tip lifts away from the sample surface by Δz (several nanometres) following the previously obtained height profile. An AC bias of 1.5 V at the resonance frequency of the cantilever was used to excite the electrical signal in the second pass, which was nullified by the DC bias servo feedback. Commercial diamond coated Si probes with a resonance frequency of ~210 kHz and a spring constant of ~72 N/m were used. The measurements were performed in air in NT-MDT pro Solver 47.

Absorption related electronic transitions in $In_xGa_{1-x}N$/GaN samples have been determined by surface photovoltage (SPV) spectroscopy measurements. SPV spectra have been acquired using the laboratory-made apparatus described in ref [23] based

on a 500M SPEX spectrometer, a pre-amplifier and an SRS lock-in amplifier, while the measurement is controlled by a LabView-based software. A Xe lamp has been used to inject photons. As the impinging photon flux varies as a function of the wavelength, the SPV raw data (SPV_{raw}) have been normalized to the photon flux Φ measured by a pyroelectric sensor and plotted as a function of the photon energy hv as follows:

$$SPV_{norm} = \frac{SPV_{raw}}{\Phi/_{hv}} \qquad (2)$$

The penetration depth of the photon beam within the samples can be estimated as α^{-1}, where α is the absorption coefficient and it varies as a function of the photon energy. Experimental values of α (red curve) and α^{-1} (black line) of $In_xGa_{1-x}N$ as a function of the photon energy, obtained by ellipsometry measurements [24], are shown in fig. 1a. It can be noticed that, for photon energies $hv \gg E_{g,GaN}$, α^{-1} becomes lower than 100 nm, thus photon absorption occurs mainly in the $In_xGa_{1-x}N$ top layer, whose thickness is 50 nm; when $hv \geq E_{g,GaN}$, absorption occurs mainly at the $In_xGa_{1-x}N$/GaN interface; while, when $hv < E_{g,GaN}$, absorption takes place mainly in the GaN buffer layer, thus in this spectral range SPV measurements are sensitive to defect-related electronic transitions in the GaN buffer layer.

3. Results

3.1 Surface potential maps.

3.1.1 Surface Morphology.

The band structure of the $In_xGa_{1-x}N$/GaN interface of Si-doped set has been simulated by numerically solving self-consistently Schrödinger-Poisson equations (NEXTNANO software [25]), with $In_xGa_{1-x}N$ and GaN offsets extracted from literature [26]. Fig 1b shows the band simulation for samples dA and dB, where sample dB is shown as representative as for all the other samples of this set, as they show similar simulated band diagrams. The difference between the band diagrams

of dA and dB is related to the fact that dA is the only fully strained sample, while the others are partially relaxed (see Table 1). Similar results have been obtained by the authors of ref [27]. A higher surface barrier height is obtained for fully strained structure and should be related to the strain-induced negative piezoelectric polarization charge density (as high as $2x10^{13}$ e/cm^2) at the interface, which widens the depletion layer.

Figure 2 (a-e) shows the surface morphology over a 5x5 μm^2 scan area for Si doped samples (from dA to dE) with different indium contents. In all the maps, apart from sample dA (fig 2a), lines running across each other at 60°are clearly visible, and from our analysis they are related to misfit dislocations at the interface creating a crosshatch pattern parallel to the surface [28]. Occurrence of such a crosshatch pattern is due to the strain relaxation in compressively strained heterostructures with hexagonal lattice via dislocation slip on <11-23>{11-22} systems towards the interface. As a result, dislocation lines running along <1-100> with a Burgers vector of a+c or 1/3<11-23> are expected, which were also observed here by TEM images [28]. The contrast for the crosshatch pattern is mainly due to preferential growth along the dislocation line on the steps formed during <11-23>{11-22} slips, which could indicate alteration in growth dynamics. In contrast to what was observed in fig 2 (b-e), fig 2a does not show any evidence of the misfit dislocation pattern, as sample dA, whose In% is below 17%, can be considered fully strained. The root mean square surface roughness has been extracted and plotted as a function of indium content in Figure 2f. The roughness increases with the indium content in correlation with the increase in the underlying crosshatch pattern density. In the roughness estimation, features of higher height, most likely related to indium droplets or localized In-rich $In_xGa_{1-x}N$ overgrowth regions, were not accounted for. The results reported here clearly show the important role of dislocations in strain relaxation and the impact of In on the degradation of the morphological properties of the layers.

3.1.2 Undoped $In_xGa_{1-x}N$ layers (x<0.18): low- and high-density V-defects

Surface electronic properties were analysed by KPFM, as the detection of work function variation could provide insight into alloy inhomogeneity, band bending and surface charge state and distribution. It was implemented on the as-grown undoped sample (uG) straight after its growth without following any surface treatment (for example, native oxide etch). The analysis broadly categorized V-defects into two types; the ones that are related to underlying threading dislocations with a higher density (HD) and the others occurring with a lower density (LD). As seen in the figures 3a and b, they are both associated with positive CPD variation across their cores forming a peak (HD V-defect is indicated by green arrow, LD V-defect by blue arrow in the figure), but they can be distinguished from the difference in the CPD values. This is evidently depicted in the CPD and height profiles comparison across the two types of V-defects in figure 3c. For the HD V-defects occurring with an aerial density ~$2x10^8$ cm^{-2}, net CPD increase at the core on average is around 20 mV and for the LD V-defects with density ~ $1x10^6$ cm^{-2}, it can go as high as 0.24 V. An aerial density in the order of $8/cm^2$ reflects the first type of V-defects (HD V-defects) are associated to TDs, which were also confirmed by TEM analyses, [29]. However, the source of second type of V-defects (LD V-defects) whose density is two order of magnitude lower, remains unclear. For a better clarity over the distribution of LD V-defects, CPD map over a scan area of 20x20 μm^2 is presented in figure 4a. Very importantly, the positive CPD variation across V-defects, which correspond to a negative variation of the work function, here suggests negatively charged space charge region across the underlying TDs or its core. This could be an evidence of positively charged core of V-defects in n-type III-nitrides. Even though it is commonly accepted that extended defects like dislocations are negatively charged in n-type GaN and positively charged only in p-type GaN [30], our observations can be understood considering a huge polarization field at $In_xGa_{1-x}N$/GaN interface and thin $In_xGa_{1-x}N$ layer which have implications on the position of the Fermi level. For undoped heterostructures, in the absence of screening, the Fermi level is very close to the valence band and could even go below the valence band near the interface,

making the neighboring region in $In_xGa_{1-x}N$ heavily or degenerate p-type. This renders the formation of donor vacancies, such as V_N, highly favorable including at the dislocation core, thus making it positively charged. This is only true for the lower segment of the V-defect (i.e. dislocation) present exclusively in $In_xGa_{1-x}N$ close to the interface while GaN remains depleted near the interface.

A rough estimation of the dimension of TD segment in a V-defect in $In_xGa_{1-x}N$ layer can be done: with the diameter of V-defects opening at the surface in the range of 50-60 nm as measured by AFM and with the $In_xGa_{1-x}N$ layer thickness of 50nm, their expected dislocation segment length is very small, $l_{TD,InGaN}$ ~ 1 to 7 nm . We also noted that any surface treatment (HCl, 2%HF or Aqua regia) for oxide etch resulted in the widening of the V-defect because of the preferential etching of semi-polar facets of V-defects, reducing $l_{TD,InGaN}$ even further with most of the lengths being reduced to 0 nm. After the oxide etch step, this positive CPD contrast related to V-defect was not observed anymore, which could be ascribed either to the diffusion of negatively charged ions (Cl^- or F^-) to the core or to the etching of a significant part of the dislocation in $In_xGa_{1-x}N$ layer. This is visible in the surface morphology in figure 3d and in the height profile across one of the V-defects. However, KPFM analysis instead showed negatively charged V-defects for such treated-surfaces. This is evident from the CPD map in figure 3e, where for each V-defect a significant local drop in CPD forming dark spots is seen, but with varying magnitudes. Across one such V-defect, a net CPD drop of ~130 mV dispersed over ~380 nm is measured in the CPD profile (figure 3e). We attribute this to be the sign of widely accepted negatively charged dislocation in n-type GaN.

The positively charged high-density and low-density V-defects were observed only in sample uG. As-grown sample uF with lower indium concentration exhibited HD V-defects with no distinguishable contrast in CPD map and LD defects with higher CPD values, where the latter type of defects were associated to trench-like defects (encircled in topography/CPD map presented in fig. 4b/c) instead of V-shape

defects unlike sample uG. The HD V-defects appeared negatively charged only after chemical treatment.

3.1.3 Doped $In_xGa_{1-x}N$ layers ($0.19 \leq x \leq 0.22$): Low density V-defects

In addition to MDs for doped sample dB, defects with a density of ~ $1x10^6$ cm^{-2} (estimated over 40x40 μm^2) were clearly detected in the CPD map as patches with dark contrast (fig. 4f). Magnified topography centered over such defects in fig. 4g reveals them to be localized over microscale circular regions (referred to as "ring-like defect" from here onwards) with diameters up to ~500 nm and are associated to a net drop in CPD value of 0.22 to 0.25 V at the core. As shown in fig 4g, this ring-like defect constitutes a well-defined ring structure elevated in Z height by ~2.7 nm and encloses a V-pit at its center. The broad radial CPD dispersion extending by more than 2 μm from its core suggests these defects are negatively charged. This behavior is reasonable for extended defects acting as electron acceptors for a heavily doped n-type $In_xGa_{1-x}N$ layer. As sample dB has a high In-content (19%), ring-like structure could be due to a local increase of indium content leading to enhanced growth over pre-existing defects of the GaN template. Though both increase in electron affinity at the V-defect {1-101} facets [[31]] and enhanced indium-inclusion in ring-like defect could as well lead to a higher work function [32], their impact on work function spatial distribution around the defect is expected to be localized and limited within the spatial resolution of the measurement technique itself. It is important to note that one must be careful in considering such an increase in the work function equivalent to the spontaneous energy barrier formation due to enhanced indium inclusion often reported for $In_xGa_{1-x}N$/GaN super lattice at V-defects [33][34].

To gain physical insight on the origin of LD defects, GaN template used in the growth of these heterostructures was investigated. Its surface morphology also shows LD V-defects with a density in the range 0.7-1.5x 10^6 cm^{-2} (estimated on area 400 - 3600 μm^2) with diameter varying between 280 to 410 nm (see figure 4h). The density and diameter obtained here are in very good agreement with the ring-like defect in the doped sample. In addition, KPFM analysis also associates these V-

defects with CPD lower than 0.7 V on average with respect to its surrounding (figure 4i), suggesting them to be negatively charged as well. These V-shape defects are most likely to be formed over underlying nano-pipes [35] and/or wide open-core screw dislocations, which are commonly occurring defects in GaN buffer [36][37][38]. In our previous work, we as well observed evidence of nanopipes in the GaN template used for growth of undoped $In_xGa_{1-x}N$ layer in the TEM analysis, however, their density assessment was not possible [29]. Similar low-density values for screw dislocations were obtained by Massabuau et al. in $In_xGa_{1-x}N$(x=0.08)/n-GaN heterostructures[39].

The CPD contrast is prominent at ring-like defects only in the case of heavily doped n-type $In_xGa_{1-x}N$ case, this could be due to Fermi-level pinning at these defects acting as electron traps. Due to low interface polarization charge density arising from strain relaxation via formation of misfit dislocation, n-type free carriers diffuse from heavily doped $In_xGa_{1-x}N$ layer into GaN buffer and get trapped at nanopipes/dislocation cores, thus rendering them negatively charged. This leads to a local upward band bending in GaN at the interface and subsequently to a lower CPD around these defects, as observed.

Comparing figures 4a, c, f and i, which are at the same scale of 20x20 μm^2, KPFM contrast analysis clearly shows local regions with a comparable density corresponding to higher CPD values in undoped $In_xGa_{1-x}N$ layers at LD V-defects and at trenches (fig 4a,c), and with lower CPDs at ring-like defects in doped $In_xGa_{1-x}N$ and at nanopipes in GaN buffer layer (fig 4f,i). The formation mechanism of such defects would require a deep structural investigation by TEM. However, this study is significantly hindered by the fact that these defects occur with a very low density. Based on our statistical comparison done through surface morphology assessment and KPFM contrast analysis, one may link the origin of these peculiar defects (LD V-shape defects, trenches and even ring-like defects) to the presence of underlying nanopipes in GaN template.

3.1.4 Undoped and heavily doped $In_xGa_{1-x}N$ layers (x≥18%): Formation of misfit dislocations

Irrespective of the doping, misfit dislocations start to appear at the interface as In concentration exceeded beyond 18% in $In_xGa_{1-x}N$ for the same nominal thickness of 50 nm. Samples with misfit dislocations are shown in figures 4d-f. Figures 4d and 4e show 20 μm x 20 μm^2 topography and CPD maps, respectively, for the undoped sample uH. The crosshatch patterns forming misfit dislocations are clearly visible in both types of maps. For the Si doped sample dB, while the morphological pattern related to the MD network is present similar to the undoped case, only negligible CPD changes appear across the MDs in the CPD map (in figure 4f) unlike in sample uH. Therefore, in doped $In_xGa_{1-x}N$ layers, MDs do not create any clear contrast in CPD maps. We can relate this effect to the presence of a high carrier density (in our case, $7x10^{18}$ – $9x10^{19}$ cm^{-3}, as shown in table 1), which is comparable to (as in samples dA and dB) or significantly higher than (as in samples dC-dE) the reported Mott density of ~10^{19} cm^{-3} in GaN [13]. Such high carrier density in doped $In_xGa_{1-x}N$ layers is enough to screen the potential induced by the polarization charge at the interface irrespective of the presence or absence of misfit dislocations. Hence, the surface barrier height over the underlying MD does not strictly depend on the interface charge density and results in a poor contrast in the KPFM image.

3.2 Surface Photovoltage Spectra.

The Si doped $In_xGa_{1-x}N$/GaN samples reported in Table 1 have been investigated by SPV spectroscopy. Figure 5a shows the SPV spectra (raw data) of the doped layers, for different doping level and In content. The spectra have been acquired from the front side of the samples while the backside was grounded. As the most relevant features in an SPV spectrum occur at the energy corresponding to the band gap [23], we can relate the two main features of each spectrum in Figure 4a to the $In_xGa_{1-x}N$ and GaN energy gaps at lower and higher energies, respectively. The SPV spectra show that $In_xGa_{1-x}N$ bandgap decreases for increasing In%, ranging approximately from 2.6 to 2.9 eV; whereas the GaN related peak is located at 3.4 eV for all the

samples. The values of the $In_xGa_{1-x}N$ band gap extracted by the SPV spectra are shown as pink stars in Figure 5b, and they are compared with previous reported results [40] and calculated Vegard's law with different bowing parameters. The band gap values are in agreement with ref [24] mostly with a bowing parameter $b = 1$. The acquisition of all the spectra has been carried out with equal photon intensities, thus the comparison between the spectra shows that the intensity of the SPV measured at the $In_xGa_{1-x}N$ gap threshold decreases when the Si doping level increases, implying that the charge injection and collection efficiency degrades for high doping level. The large electron density of the highly doped layers (around 10^{20} cm^{-3}) promotes recombination with photo-generated holes, decreasing the overall signal.

In addition to the band-gap related features, the spectra in Fig. 5a show a drop of the signal around 3.3 eV, which deepens with higher Si doping. The least magnitude of the drop is seen for sample dA with lowest Si doping concentration and without MDs. The decrease of the SPV signal at photon energies just above the $In_xGa_{1-x}N$ band gap can be related to an interface recombination effect. As shown in Fig. 1a, the inverse of the absorption coefficient, which equals the light penetration depth, decreases for above band gap energies; thus, in this spectral region the SPV signal is related to recombination phenomena at the interface [20]. Therefore, high Si doping corresponds to a higher interface recombination rate, as Si incorporation induces active interface recombination centers. Moreover, both indium content and silicon doping affect the steepness of the $In_xGa_{1-x}N$ gap- related increase. An ideal peak should be a step function that rises precisely at the energy of the bandgap. In real spectra, the signal increases more gradually with a certain slope. This slope can be attributed to the formation of Urbach tails due to a disordered structure [20]. In Fig. 5a, it is visible that the slope decreases as both Si doping and In content increases; indeed, the increment of both elements concentration creates more defects, indium statistical fluctuation or alloy disorder [41],[22] and phase separation [42] leading to a more pronounced Urbach tails.

For comparison, normalized SPV spectra of the undoped $In_xGa_{1-x}N$/GaN samples uF and uH, without and with misfit dislocations, respectively, are reported in Fig. 6a. Similar to the doped samples spectra, the band gap related features at 3.4 eV (GaN) and in the range varying from 2.7 eV to 2.85 eV ($In_xGa_{1-x}N$) for both samples are visible in the spectra. However, the signals appear quite different in the transition range between the two gaps, which corresponds to the interface region. Indeed, a dip occurs in the sample uH at around 3.3 eV. The dip could be related to recombination processes occurring at the $In_xGa_{1-x}N$/GaN interface induced by MDs, while the SPV spectrum of the sample without MDs (uF) does not show a similar drop as in sample dA with least Si doping. Another feature appears in both samples in the form of a band at around 2.2- 2.4 eV in the spectra of Fig 6a. The same feature appears in the SPV spectra in fig 6b, where scans acquired from different spots on the surface of the GaN template are shown. This feature must be related to the yellow band transition (YB) which is very common in GaN and widely reported in literature and is associated to defects present near the surface [43]. It is interesting to note that this transition is not visible in the SPV spectra of the doped samples (fig. 5). This further strengthens our claim of high Si doping and strain induced recombination centers at the interface.

4. Discussion and Conclusions.

We have investigated Misfit dislocations, threading dislocations, V defects and interfaces in $In_xGa_{1-x}N$/GaN heterostructures by surface potential maps and spectra. As mentioned in the introduction section, while these extended defects have been intensively studied through structural investigation, their electron-hole recombination mechanisms are still quite debated. These mechanisms play a major role in current transport and device reliability. We summarize in the following the main results achieved, highlighting the role of In concentration and doping on the defect characteristics:

- The present analysis has allowed us to detect two categories of V-defects in $In_xGa_{1-x}N$/GaN heterostructures appearing in different densities (Low and High, LD, and HD)
- **In undoped $In_xGa_{1-x}N$/GaN heterostructures**, KPFM maps shows that HD **V defects, corresponding to threading dislocations are positively charged**, contrary to what is known for bulk n-type GaN. This is most likely to be due to the position of the Fermi-level of the $In_xGa_{1-x}N$ layer near the interface with GaN, which is very close to the valence band.
- **In partially relaxed $In_xGa_{1-x}N$ layers**, as observed by KPFM, misfit dislocations are associated to a local drop in work function values, thus MDs create potential wells where electron-hole recombination phenomena are enhanced. The effect of misfit dislocations in the enhancement of electron – hole recombination at the $In_xGa_{1-x}N$/GaN heterointerface is also observed by SPV spectra. WF drops at MDs are not revealed by KPFM in highly Si doped samples due to the effect of doping-induced screening.
- LD V-defects appear in AFM and KPFM maps as ring-like defects, likely related to nanopipes in the GaN buffer, they are associated to an increase in the WF values, which in turn creates a potential barrier for mobile charges. This result could explain why V-defects can have beneficial effects in $In_xGa_{1-x}N$: they can prevent electron-hole recombination, resulting in the enhancement of $In_xGa_{1-x}N$ based LED efficiency, as reported by ref [10].
- **High Si doping concentration** enhances the recombination at the hetero-interface and decreases the efficiency in mobile charge separation, as shown by SPV spectra. Lower spreading resistance in the regions around MDs suggest either preferential Si incorporation or improved dopant activation. **High In% and Si doping levels** also lead to an increase of roughness and alloy-disorder which results in large Urbach tails. Misfit dislocations as well promote local crystal disorder increasing Urbach tails.

- The energy gap of $In_xGa_{1-x}N$ has been determined as a function of the In%. The results agree with the Vegard's law with a bowing parameter close to 1.

By summarizing, very high In and Si concentrations play a major role in increasing crystal disorder and interface recombination. The doping level also affect the charge state of the defect.

The results here presented we have contributed to the clarification of defects induced carrier recombination mechanisms in $In_xGa_{1-x}N$/GaN heterostructures.

Acknowledgments

This work was supported by the EU under Project No. PITN-GA-2008-213238 (RAINBOW). Ana Cros acknowledges financial support from project PROMETEO/2018/123 from Generalitat Valenciana and project ENE2016-79282-C5-3-R cofinanced by the Spanish MICINN and FEDER.

Literature

[1] T. Lin, Z.Y. Zhou, Y.M. Huang, K. Yang, B.J. Zhang, Z.C. Feng, Strain-Controlled Recombination in InGaN/GaN Multiple Quantum Wells on Silicon Substrates, Nanoscale Res. Lett. 13 (2018). doi:10.1186/s11671-018-2663-6.

[2] U.K. Mishra, P. Parikh, Y.F. Wu, AlGaN/GaN HEMTs - An overview of device operation and applications, Proc. IEEE. 90 (2002) 1022–1031. doi:10.1109/JPROC.2002.1021567.

[3] H. Kurokawa, M. Kaga, T. Goda, M. Iwaya, T. Takeuchi, S. Kamiyama, I. Akasaki, H. Amano, Multijunction GaInN-based solar cells using a tunnel junction, Appl. Phys. Express. 7 (2014) 034104. doi:10.7567/APEX.7.034104.

[4] K. Safa, P. Capper, Springer Handbook of Electronic and Photonic Materials, 2014. doi:10.1007/s13398-014-0173-7.2.

[5] Y. Chen, T. Takeuchi, H. Amano, I. Akasaki, N. Yamada, Y. Kaneko, S.Y. Wang, Pit formation in GaInN quantum wells, Appl. Phys. Lett. 72 (1998) 710–712.

doi:10.1063/1.120853.

[6] S.C. Tsai, M.J. Li, H.C. Fang, C.H. Tu, C.P. Liu, Efficiency enhancement of blue light emitting diodes by eliminating V-defects from InGaN/GaN multiple quantum well structures through GaN capping layer control, Appl. Surf. Sci. 439 (2018) 1127–1132. doi:10.1016/j.apsusc.2018.01.074.

[7] S. Srinivasan, L. Geng, R. Liu, F.A. Ponce, Y. Narukawa, S. Tanaka, Slip systems and misfit dislocations in InGaN epilayers, Appl. Phys. Lett. 83 (2003) 5187–5189. doi:10.1063/1.1633029.

[8] J. Moneta, M. Siekacz, E. Grzanka, T. Schulz, T. Markurt, M. Albrecht, J. Smalc-Koziorowska, Peculiarities of plastic relaxation of (0001) InGaN epilayers and their consequences for pseudo-substrate application, Appl. Phys. Lett. 113 (2018). doi:10.1063/1.5030190.

[9] C. Haller, J.F. Carlin, G. Jacopin, D. Martin, R. Butté, N. Grandjean, Burying non-radiative defects in InGaN underlayer to increase InGaN/GaN quantum well efficiency, Appl. Phys. Lett. 111 (2017). doi:10.1063/1.5007616.

[10] H.Y. Shih, M. Shiojiri, C.H. Chen, S.F. Yu, C.T. Ko, J.R. Yang, R.M. Lin, M.J. Chen, Ultralow threading dislocation density in GaN epilayer on near-strain-free GaN compliant buffer layer and its applications in hetero-epitaxial LEDs, Sci. Rep. 5 (2015) 1–11. doi:10.1038/srep13671.

[11] S. Zhou, X. Liu, H. Yan, Y. Gao, H. Xu, J. Zhao, Z. Quan, C. Gui, S. Liu, The effect of nanometre-scale V-pits on electronic and optical properties and efficiency droop of GaN-based green light-emitting diodes, Sci. Rep. 8 (2018) 1–12. doi:10.1038/s41598-018-29440-4.

[12] D.H. Kim, Y.S. Park, D. Kang, K.K. Kim, T.Y. Seong, H. Amano, Combined effects of V pits and chip size on the electrical and optical properties of green InGaN-based light-emitting diodes, J. Alloys Compd. 796 (2019) 146–152. doi:10.1016/j.jallcom.2019.05.070.

[13] D.N. Nath, E. Gür, S.A. Ringel, S. Rajan, Molecular beam epitaxy of N-polar InGaN, Appl. Phys. Lett. 97 (2010) 071903. doi:10.1063/1.3478226.

[14] J.W.P. Hsu, H.M. Ng, A.M. Sergent, S.N.G. Chu, Scanning Kelvin force microscopy imaging of surface potential variations near threading dislocations in GaN, Appl. Phys. Lett. 81 (2002) 3579–3581. doi:10.1063/1.1519732.

[15] B.J. Rodriguez, W.-C. Yang, R.J. Nemanich, A. Gruverman, Scanning probe investigation of surface charge and surface potential of GaN-based heterostructures, Appl. Phys. Lett. 86 (2005) 112115. doi:10.1063/1.1869535.

[16] M. Foussekis, J.D. McNamara, A.A. Baski, M.A. Reshchikov, Temperature-dependent Kelvin probe measurements of band bending in *p* -type GaN, Appl. Phys. Lett. 101 (2012) 082104. doi:10.1063/1.4747203.

[17] A. Minj, H. Ben Ammar, A. Cros, N. Garro, P. Gamarra, S.L. Delage, P. Ruterana, Probing the Local Electrical Properties of Al(In,Ga)N by Kelvin Probe Force Microscopy, Phys. Status Solidi Basic Res. 255 (2018) 1–6. doi:10.1002/pssb.201700427.

[18] O Tuna, Understanding and Optimization of InN and high Indium containing InGaN alloys by Metal Organic Chemical Vapor Deposition, Aachen, 2013. https://inis.iaea.org/search/search.aspx?orig_q=RN:45042262.

[19] M. Nonnenmacher, M.P. O'Boyle, H.K. Wickramasinghe, Kelvin probe force microscopy, Appl. Phys. Lett. 58 (1991) 2921–2923. doi:10.1063/1.105227.

[20] L. Kronik, Y. Shapira, Surface photovoltage phenomena: Theory, experiment, and applications, Surf. Sci. Rep. (1999). doi:10.1016/S0167-5729(99)00002-3.

[21] D. Holec, P.M.F.J. Costa, M.J. Kappers, C.J. Humphreys, Critical thickness calculations for InGaN/GaN, J. Cryst. Growth. 303 (2007) 314–317. doi:10.1016/j.jcrysgro.2006.12.054.

[22] A. Minj, M.F. Romero, Y. Wang, Tuna, M. Feneberg, R. Goldhahn, G. Schmerber, P. Ruterana, C. Giesen, M. Heuken, Stimulated emission via electron-hole plasma recombination in fully strained single InGaN/GaN heterostructures, Appl. Phys. Lett. 109 (2016). doi:10.1063/1.4968799.

[23] D. Cavalcoli, M.A. Fazio, Electronic transitions in low dimensional semiconductor structures measured by surface photovoltage spectroscopy,

Mater. Sci. Semicond. Process. 92 (2019) 28–38. https://www.sciencedirect.com/science/article/pii/S1369800118304177.

[24] S.A. Kazazis, E. Papadomanolaki, M. Androulidaki, M. Kayambaki, E. Iliopoulos, Optical properties of InGaN thin films in the entire composition range, J. Appl. Phys. 123 (2018). doi:10.1063/1.5020988.

[25] nextnano, (n.d.). https://www.nextnano.de/.

[26] L. Dong, First Principles Study of Band Offsets and Band Bending of InxGa1-xN / GaN and Zn1-xBexO / ZnO Heterostructures and Quantum Wells, University of Connecticut Graduate School, 2013.

[27] X. Sun, X. Wang, S. Liu, P. Wang, D. Wang, X. Zheng, L. Sang, M. Sumiya, S. Ueda, M. Li, J. Zhang, W. Ge, B. Shen, Determination of the transition point from electron accumulation to depletion at the surface of in<inf>x</inf>Ga<inf>1-</inf><inf>x</inf>N films, Appl. Phys. Express. 11 (2018). doi:10.7567/APEX.11.021001.

[28] Q.T. Li, A. Minj, M.P. Chauvat, J. Chen, P. Ruterana, Interface dislocations in InxGa1–xN/GaN heterostructures, Phys. Status Solidi Appl. Mater. Sci. 214 (2017) 1–5. doi:10.1002/pssa.201600442.

[29] A. Minj, D. Cavalcoli, G.R. Mutta Popuri, A. Vilalta-Clemente, P. Ruterana, A. Cavallini, Electrical properties of extended defects in III-nitrides, Acta Mater. 89 (2015) 290–297. doi:10.1016/j.actamat.2015.01.061.

[30] D. Cherns, C.G. Jiao, Electron Holography Studies of the Charge on Dislocations in GaN, Phys. Rev. Lett. 87 (2001) 205504. doi:10.1103/PhysRevLett.87.205504.

[31] A.L. Rosa, J. Neugebauer, First-principles calculations of the structural and electronic properties of clean GaN (0001) surfaces, Phys. Rev. B. 73 (2006) 205346. doi:10.1103/PhysRevB.73.205346.

[32] P.G. Moses, M. Miao, Q. Yan, C.G. Van de Walle, Hybrid functional investigations of band gaps and band alignments for AlN, GaN, InN, and InGaN, J. Chem. Phys. 134 (2011) 084703. doi:10.1063/1.3548872.

[33] A. Hangleiter, F. Hitzel, C. Netzel, D. Fuhrmann, U. Rossow, G. Ade, P. Hinze, Suppression of Nonradiative Recombination by V-Shaped Pits in GaInN / GaN Quantum Wells Produces a Large Increase in the Light Emission Efficiency, Phys. Rev. Lett. 95 (2005) 127402. doi:10.1103/PhysRevLett.95.127402.

[34] A. Kaneta, M. Funato, Y. Kawakami, Nanoscopic recombination processes in InGaN/GaN quantum wells emitting violet, blue, and green spectra, Phys. Rev. B. 78 (2008) 125317. doi:10.1103/PhysRevB.78.125317.

[35] Z. Liliental-Weber, Y. Chen, S. Ruvimov, J. Washburn, Formation Mechanism of Nanotubes in GaN, Phys. Rev. Lett. 79 (1997) 2835–2838. doi:10.1103/PhysRevLett.79.2835.

[36] W. Qian, G.S. Rohrer, M. Skowronski, K. Doverspike, L.B. Rowland, D.K. Gaskill, Open-core screw dislocations in GaN epilayers observed by scanning force microscopy and high-resolution transmission electron microscopy, Appl. Phys. Lett. 67 (1995) 2284–2286. doi:10.1063/1.115127.

[37] I. Arslan, N.D. Browning, Role of Oxygen at Screw Dislocations in GaN, Phys. Rev. Lett. 91 (2003) 165501. doi:10.1103/PhysRevLett.91.165501.

[38] S. Usami, N. Mayama, K. Toda, A. Tanaka, M. Deki, S. Nitta, Y. Honda, H. Amano, Direct evidence of Mg diffusion through threading mixed dislocations in GaN p–n diodes and its effect on reverse leakage current, Appl. Phys. Lett. 114 (2019) 232105. doi:10.1063/1.5097767.

[39] F.C.P. Massabuau, P. Chen, M.K. Horton, S.L. Rhode, C.X. Ren, T.J. O'Hanlon, A. Kovács, M.J. Kappers, C.J. Humphreys, R.E. Dunin-Borkowski, R.A. Oliver, Carrier localization in the vicinity of dislocations in InGaN, J. Appl. Phys. 121 (2017). doi:10.1063/1.4973278.

[40] S. Pandey, D. Cavalcoli, A. Cavallini, Band bowing and Si donor levels in InGaN layers investigated by surface photo voltage spectroscopy, Appl. Phys. Lett. 102 (2013) 142101. doi:10.1063/1.4799658.

[41] M. Auf der Maur, A. Pecchia, G. Penazzi, W. Rodrigues, A. Di Carlo, Efficiency

Drop in Green InGaN / GaN Light Emitting Diodes: The Role of Random Alloy Fluctuations, Phys. Rev. Lett. 116 (2016) 027401. doi:10.1103/PhysRevLett.116.027401.

[42] P. Ruterana, F. Deniel, Observation of ordering and phase separation in InxGa1−xN layers, Mater. Sci. Eng. B. 59 (1999) 186–190. doi:10.1016/S0921-5107(98)00408-5.

[43] M.A. Reshchikov, J.D. McNamara, H. Helava, A. Usikov, Y. Makarov, Two yellow luminescence bands in undoped GaN, Sci. Rep. 8 (2018) 1–11. doi:10.1038/s41598-018-26354-z.

[44] W. Shan, W. Walukiewicz, J. Wu, K.M. Yu, J.W. Ager, S.X. Li, E.E. Haller, J.F. Qeisz, D.J. Friedman, S.R. Kurtz, Band-gap bowing effects in BxGa1-xAs alloys, J. Appl. Phys. 93 (2003) 2696–2699. doi:10.1063/1.1540230.

[45] J. Wu, W. Walukiewicz, K.M. Yu, J.W. Ager, E.E. Haller, H. Lu, W.J. Schaff, Y. Saito, Y. Nanishi, Unusual properties of the fundamental band gap of InN, Appl. Phys. Lett. 80 (2002) 3967–3969. doi:10.1063/1.1482786.

[46] I. Gorczyca, T. Suski, N.E. Christensen, A. Svane, Size effects in band gap bowing in nitride semiconducting alloys, Phys. Rev. B. 83 (2011) 153301. doi:10.1103/PhysRevB.83.153301.

Figure Captions

Figure 1. a) Measured $In_xGa_{1-x}N$ absorption coefficient α (blue curve) and penetration depth α^{-1} (black curve) vs. photon energy. b) Band simulations at the $In_xGa_{1-x}N$/GaN interface for doped sample dA (In content 14%, fully strained) and doped sample dB (In content 19%, relaxed).

Figure 2. Morphology maps of Si doped $In_xGa_{1-x}N$/GaN samples a) dA, 14% In, b) dB, 19% In c) dC, 22.0% In d) dD 19.3% In and e) dE 19.3% In. f) Roughness extracted from the morphology maps. The orange curve is a guide for the eye.

Figure 3. Surface morphologies (a, d) and their corresponding CPD maps (b, e) of the as-grown and oxide-etched undoped sample uG, respectively. (c, f) Similarly, height and CPD profiles across three V-defects (two HD V-defects indicated in green arrow and 1 LD V-defect in blue) for as-grown and a single V-defect for as-grown and oxide-etched sample. Two LD and one HD V-defects are encircled as well for better clarity. The height profile does not pass through the second HD V-defect and therefore it is not indicated in green arrow.

Figure 4. Comparative CPD maps over 20x20 μm^2 scan area of undoped samples uG (a) and uF (c) without MDs, and uH (e) with MDs, doped sample dB (f) and GaN template used for growth (i). Respective topographies (b, d, h) displayed on the left of the CPD maps (c, e, i) correspond to samples uF, uH and GaN template. GaN morphology shows small V-pits and large V-pits. The small V-pits are indicated by green arrows. (g) Surface morphology (left), CPD map (right) and CPD/Height profiles across a ring-like defect indicated in dashed line. MD line directions along the three <1-100> directions are indicated in (d) and (f).

Figure 5. a) SPV spectra acquired by Xe lamp of Si doped $In_xGa_{1-x}N$/GaN samples (see Table 1) from front of the structure. b) Calculated energy gap values of $In_xGa_{1-x}N$ layers for different bowing parameters (lines) and our new results (pink stars) compared with earlier reported results in: [44][45][46][40][24].

Figure 6. a) Normalised spectra of samples uH (black line) and uF (orange line) as a function of photon energy. b) GaN buffer layer normalised spectra acquired in different spots of the surface.

Figure
Click here to download high resolution image

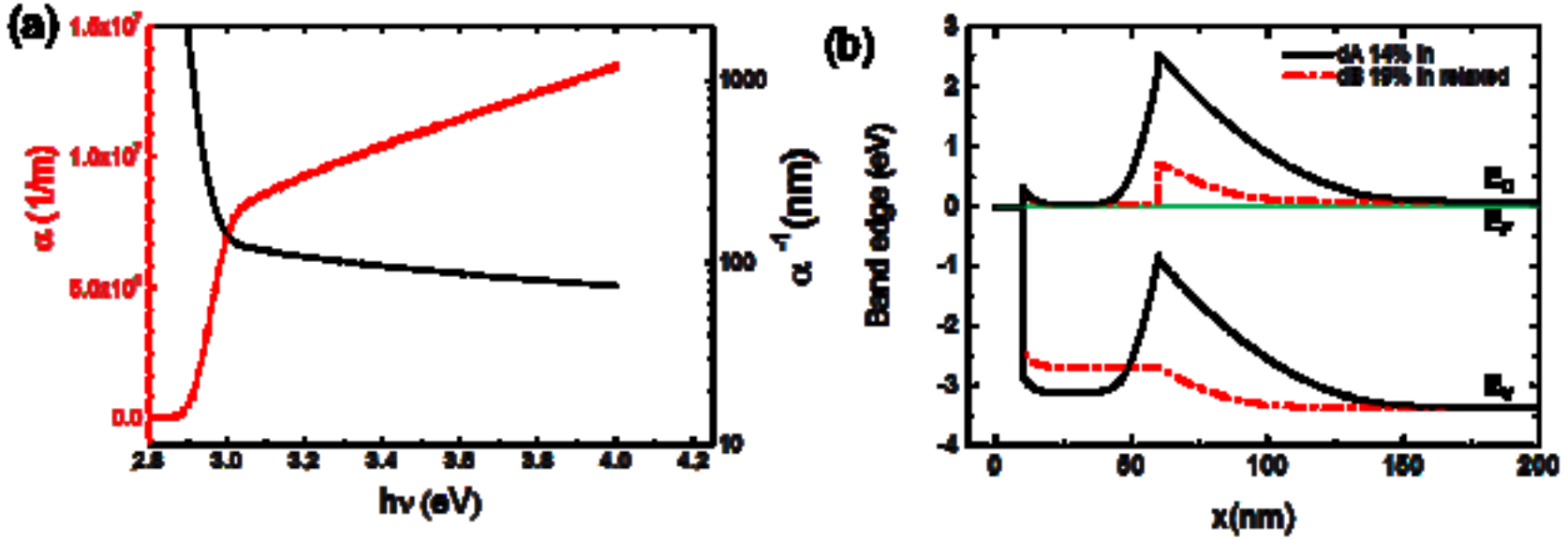

Figure 1: Figure 1. a) Measured $In_xGa_{1-x}N$ absorption coefficient α (blue curve) and penetration depth α^{-1} (black curve) vs. photon energy. b) Band simulations at the $In_xGa_{1-x}N$/GaN interface for samples dA (In content 14%, fully strained) and dB (In content 19%, if relaxed).

Figure2
Click here to download high resolution image

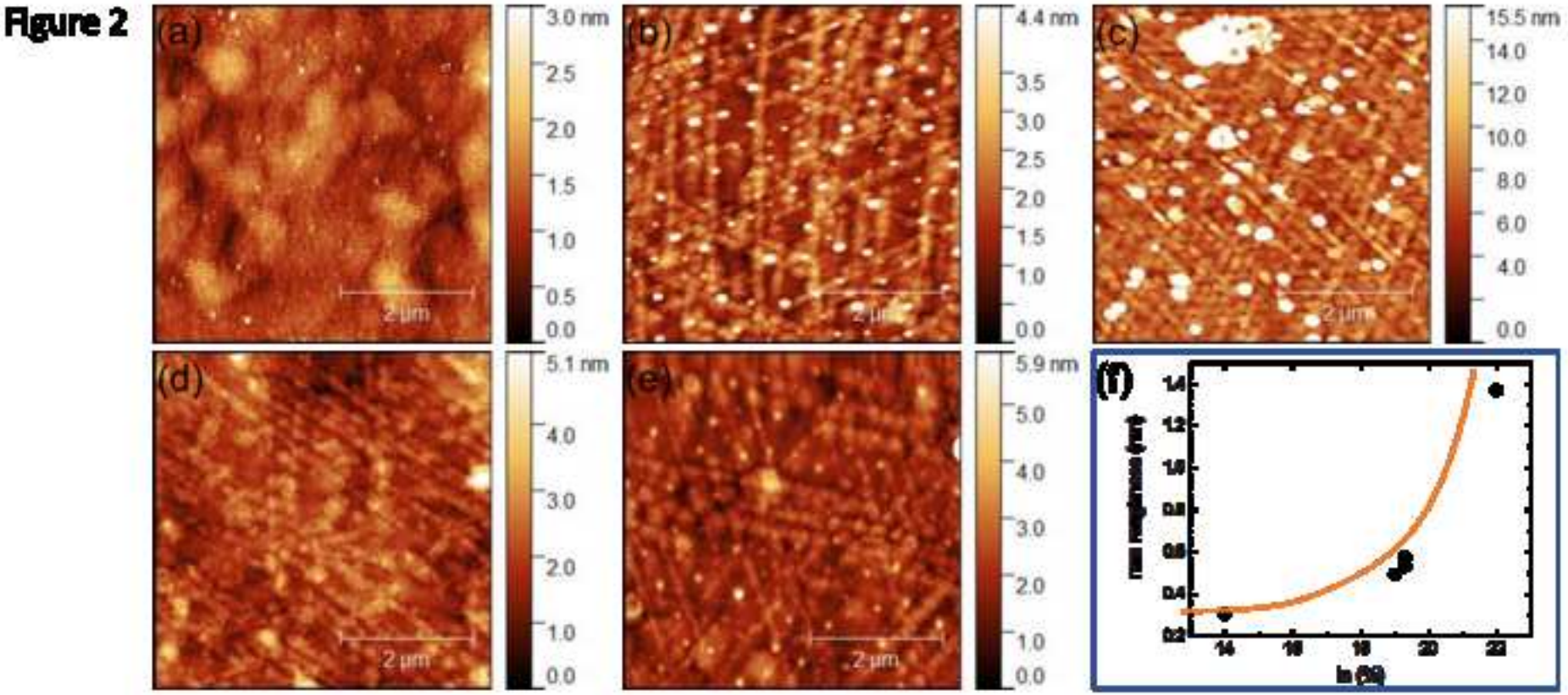

Figure 2. Morphology maps of Si doped $In_xGa_{1-x}N$/GaN samples a) dA, 14% In, b) dB, 19% In c) dC, 22.0% In d) dD 19.3% In and e) dE 19.3% In. f) Roughness extracted from the morphology maps. The orange curve is a guide for the eye.

Figure3
Click here to download high resolution image

Figure 3

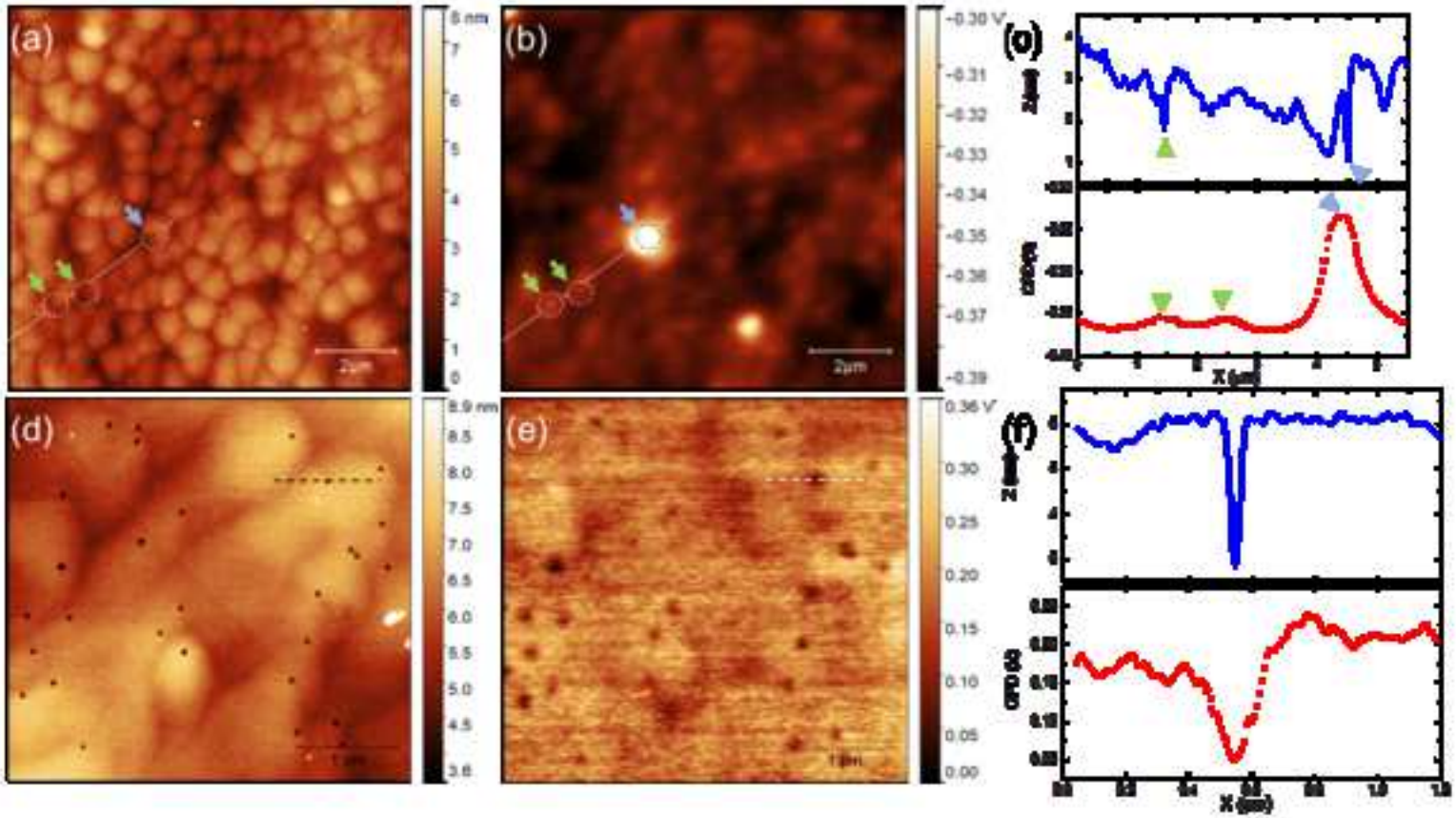

Figure 3. Figure 9. Surface morphologies (a, d) and their corresponding CPD maps (b, e) of the as-grown and oxide-etched undoped sample uG, respectively. (c, f) Similarly, height and CPD profiles across three V-defects (two HD V-defects indicated in green arrow and 1 LD V-defect in blue) for as-grown and a single V-defect for as-grown and oxide-etched sample. Two LD and one HD V-defects are encircled as well for better clarity. The height profile does not pass through the second HD V-defect and therefore it is not indicated in green arrow.

Figure4
Click here to download high resolution image

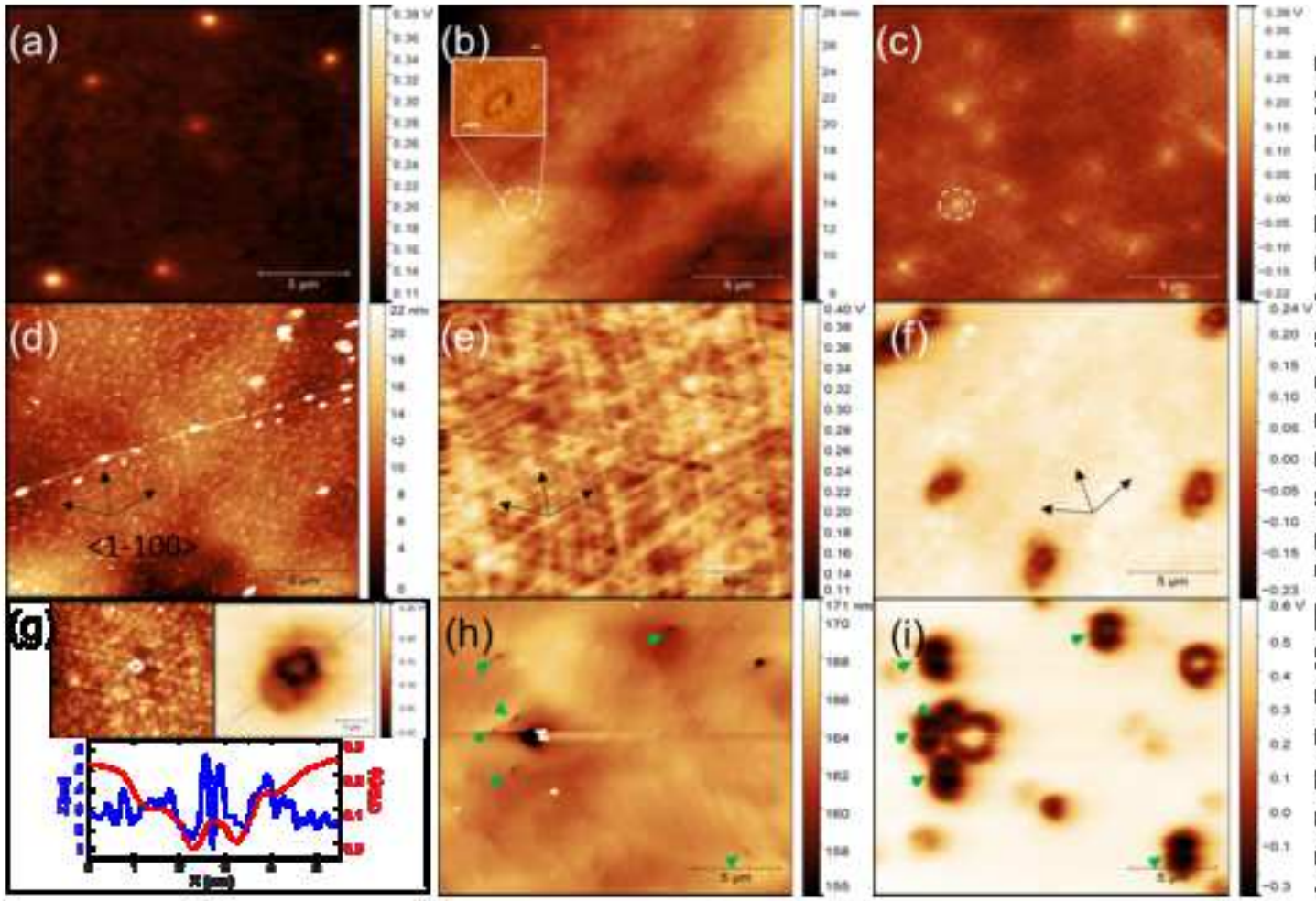

FIG4

Comparative CPD maps over 20x20 μm² scan area of undoped samples uG (a) and uF (c) without MDs, and uH (e) with MDs, doped sample dB (f) and GaN template used for growth (i). Respective topographies (b, d, h) displayed on the left of the CPD maps (c, e, i) correspond to samples uF, uH and GaN template. GaN morphology shows small V-pits and large V-pits. The small V-pits are indicated by green arrows. (g) Surface morphology (left), CPD map (right) and CPD/Height profiles across a ring-like defect indicated in dashed line. MD line directions along the three <1-100> directions are indicated in (d) and (f).

Figure5
Click here to download high resolution image

Figure 5

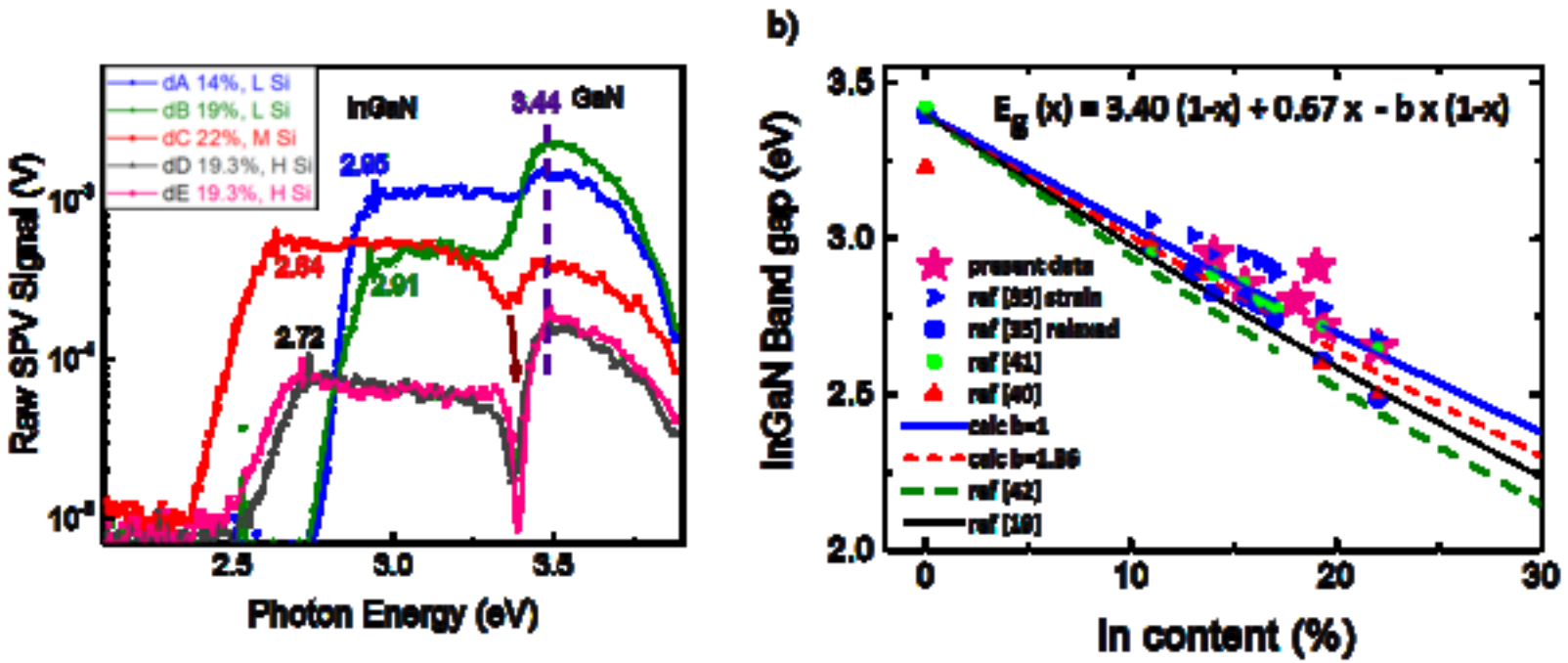

Figure 5. a) SPV spectra acquired by Xe lamp of Si doped $In_xGa_{1-x}N$/GaN samples (see Table 1) from front of the structure. b) Calculated energy gap values of $In_xGa_{1-x}N$ layers for different bowing parameters (lines) and our new results (pink stars) compared with earlier reported results in: [40][41][42][35][19].

Figure6
Click here to download high resolution image

Figure 6

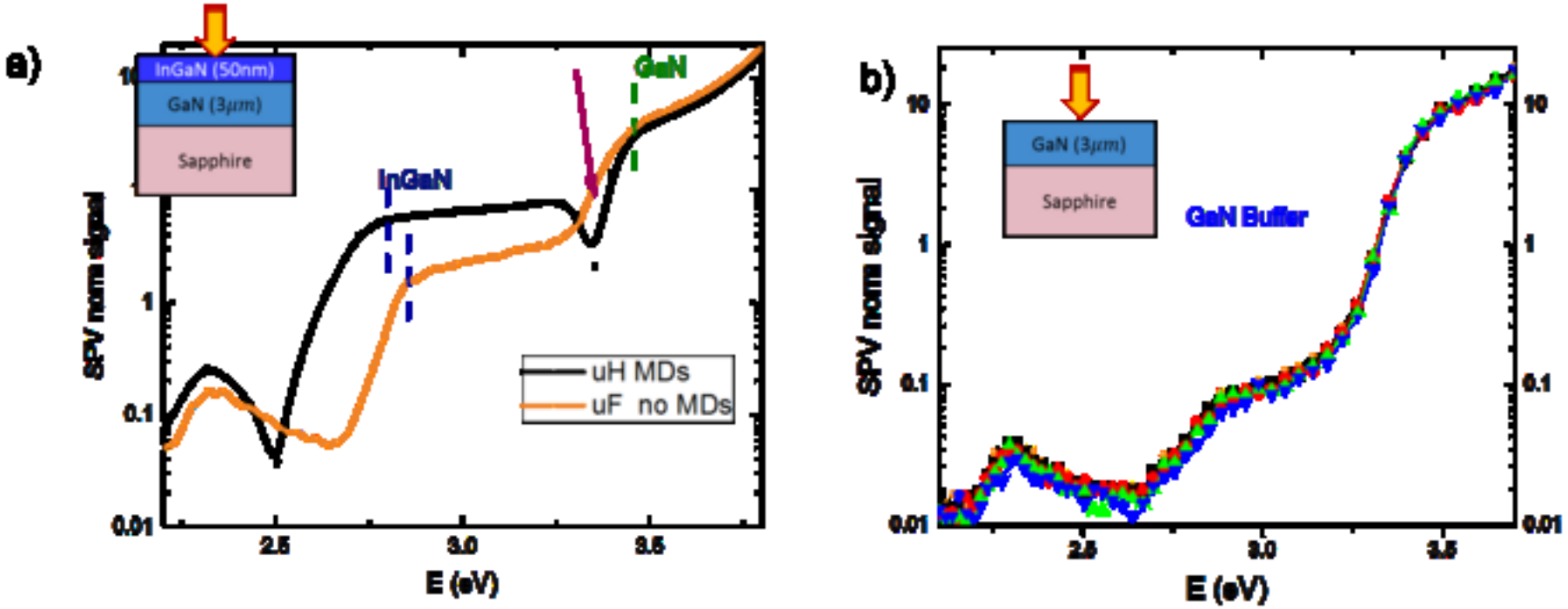

Figure 6. a) Normalised spectra of samples uH (black line) and uF (orange line) as a function of photon energy. b) GaN buffer layer normalised spectra acquired in different spots of the surface.

***Declaration of Interest Statement**

Declaration of interests

✕ The authors declare that they have no known competing financial interests or personal relationships that could have appeared to influence the work reported in this paper.

☐The authors declare the following financial interests/personal relationships which may be considered as potential competing interests:

On behalf of the Authors
Prof Daniela Cavalcoli

CREDIT Author statement

Daniela Cavalcoli Daniela.cavalcoli@unibo.it, corresponding Author, contributed to: Conceptualization and Writing - Review, Editing and supervision

Albert Minj: albert.minj@kuleuven.be, contributed to Conceptualization, investigations, and Writing - Review & Editing

Maria Antonietta Fazio: maria.fazio2@unibo.it contributed to investigations and Writing - Original Draft

Ana Cros: Ana.Cros@uv.es contributed to Review, Editing and supervision.

Michel Heuken: M.Heuken@aixtron.com contributed to: Review, Editing and supervision.